

This discussion paper is/has been under review for the journal Atmospheric Chemistry and Physics (ACP). Please refer to the corresponding final paper in ACP if available.

Global modeling of SOA: the use of different mechanisms for aqueous phase formation

G. Lin¹, S. Sillman¹, J. E. Penner¹, and A. Ito²

¹Department of Atmospheric, Oceanic, and Space Sciences, University of Michigan, Ann Arbor, Michigan, USA

²Research Institute for Global Change, JAMSTEC, Yokohama, Kanagawa, 236-0001, Japan

Received: 2 November 2013 – Accepted: 4 November 2013 – Published: 12 November 2013

Correspondence to: G. Lin (gxlin@umich.edu)

Published by Copernicus Publications on behalf of the European Geosciences Union.

Title Page

Abstract

Introduction

Conclusions

References

Tables

Figures

◀

▶

◀

▶

Back

Close

Full Screen / Esc

Printer-friendly Version

Interactive Discussion



Abstract

There is growing interest in the formation of secondary organic aerosol (SOA) through condensed aqueous phase reactions. In this study, we use a global model (IMPACT) to investigate the potential formation of SOA in the aqueous phase. We compare results from several multiphase process schemes with detailed aqueous phase reactions to schemes that use a first order gas-to-particle formation rate based on uptake coefficients. The net global SOA production rate in cloud water ranges from 19.5 Tgyr^{-1} to 46.8 Tgyr^{-1} while that in aerosol water ranges from -0.9 Tgyr^{-1} to 12.6 Tgyr^{-1} . The rates using first order uptake coefficients are over two times higher than the multiphase schemes in cloud water. Using first order uptake coefficients leads to a net SOA production rate in aerosol water as high as 12.6 Tgyr^{-1} , while the fully multiphase schemes cause a negative net production rate. These rates can be compared to the gas phase formation rate of 29.0 Tgyr^{-1} that results from gas-particle partitioning and the formation rate of 25.8 Tgyr^{-1} from the uptake of epoxide. The annual average organic acid concentrations (the major SOA products formed in cloud) peak over the tropical regions, while oligomers (the major SOA products formed in aerosol water) generally show maxima over industrialized areas in the Northern Hemisphere. A sensitivity test to investigate two representations of cloud water content from two global models shows that increasing cloud water by a factor of 2.7 can increase the net SOA production rate in cloud by a factor of 4.2 at low altitudes (below approximately 900 hPa). We also investigated the importance of including dissolved iron chemistry in cloud water aqueous reactions. Adding these reactions increases the formation rate of aqueous phase HO_x by a factor of 2.2 and decreases the amount of global SOA formed by 44 %. Previously, we showed that the model that uses the uptake method to simulate SOA formed in both cloud and aerosol water over-predicts observed SOA by a factor as high as 3.8 in tropical regions. The use of the multiphase reaction scheme for SOA formation in cloud water brings the model's predictions to within a factor of 2 of the observations. All simulations show reasonable agreement with aerosol mass spectrometry (AMS) mea-

Global modeling of SOA

G. Lin et al.

[Title Page](#)[Abstract](#)[Introduction](#)[Conclusions](#)[References](#)[Tables](#)[Figures](#)[◀](#)[▶](#)[◀](#)[▶](#)[Back](#)[Close](#)[Full Screen / Esc](#)[Printer-friendly Version](#)[Interactive Discussion](#)

surements in the Northern Hemisphere, though using the uptake method to simulate SOA formed in aerosol water improves the results by around 10% compared to the use of the multiphase reaction scheme. All cases studied here tend to underestimate observations of oxalic acid, particularly in Europe in winter, in the Amazon, Africa, and China as well as over ocean regions. The model with iron chemistry under predicts measurements in almost all regions. Finally, the comparison of O/C ratios estimated in the model with those estimated from measurements shows that the modeled SOA has a slightly higher O/C ratio than the observed SOA for all cases.

1 Introduction

Secondary organic aerosol (SOA) has been shown to be an important component of non-refractory submicron aerosol in the atmosphere (Zhang et al., 2007; Jimenez et al., 2009). SOA is known to form from the gas/particle partitioning of semi-volatile organic compounds produced by gas phase photochemistry (Pankow, 1994; Odum et al., 1996). However, models that only include this SOA formation mechanism typically underestimate the SOA mass as well as the oxygen-to-carbon (O/C) ratio (e.g., DeGouw et al., 2005; Heald et al., 2005; Volkamer et al., 2006; Dzepina et al., 2009). In addition, the observed O/C ratios in aged ambient organic aerosol (OA) cannot be explained using measured O/C ratios in dry smoke chamber experiments (Aiken et al., 2008; Ng et al., 2010). Several other methods have been used to help close the gap between measured and modeled SOA. These include using a refined treatment for primary organic aerosol (POA) that allows them to evaporate and further oxidize (Robinson et al., 2007; Pye and Seinfeld, 2010; Hodzic et al., 2010; Lee-Taylor et al., 2011). However, there are large uncertainties in how to treat the evaporation rate as well as the oxidation mechanism for POA and thus the SOA yield from this source (Pye and Seinfeld, 2010; Spracklen et al., 2011).

Aqueous phase processing, as a complementary pathway to gas/particle partitioning of semi-volatile and low volatility gases, has the potential to enhance both SOA mass

Global modeling of
SOA

G. Lin et al.

Title Page

Abstract

Introduction

Conclusions

References

Tables

Figures

◀

▶

◀

▶

Back

Close

Full Screen / Esc

Printer-friendly Version

Interactive Discussion



and the O/C ratio in atmospheric OA. Water-soluble and polar gases are taken up by the aqueous phase and can be oxidized there leading to the production of low volatility substances (e.g., organic acids, oligomers, and organosulfates) (Blando and Turpin, 2000; Warneck, 2003; Liggió et al., 2005; Sorooshian et al., 2007; Tan et al., 2009);

5 These low-volatility products predominately stay in the particle phase after water evaporation (Blando and Turpin, 2000; El Haddad et al., 2009) and thereby increase SOA concentrations and tend to have higher O/C ratios than those that form in gas phase reactions (Herrmann et al., 2005; Lim et al., 2010; Ervens and Volkamer, 2010). This is because the precursors for the aqueous phase reactions tend to be small compounds with low-molecular weight (MW) that already have high O/C ratios, and the aqueous oxidation of these small compounds either tends to add O-containing functional groups to C-C bonds (thereby forming higher O/C ratio dicarboxylic acids) or to react with themselves to keep the same carbon structure and the same O/C ratio (thereby forming oligomers) (Ervens et al., 2011).

15 Laboratory studies have shown that aqueous phase reactions can produce SOA from C2 and C3 carbonyl compounds including glyoxal, methylglyoxal, glycolaldehyde, pyruvic acid and acetic acid (Ervens et al., 2003; Carlton et al., 2006, 2007; Altieri et al., 2008; Perri et al., 2009; Tan et al., 2009, 2010, 2012; Lim et al., 2010). The major products from the oxidation of these carbonyl compounds are carboxylic acids, of which the most important is oxalic acid. Oxalic acid is also observed to part of the aerosol emitted in biomass burning (Kundu et al., 2010) and is observed to be formed from the photochemical ageing of OA (Eliason et al., 2003). In contrast to reactions in cloud, the major products formed from the reactions of C2 and C3 carbonyl compounds in aerosol water are oligomers (Ervens and Volkamer, 2010; Lim et al., 2010). The oxidation of methyl vinyl ketone (MVK) and methacrolein (MACR) in the aqueous phase can be an additional source for SOA formation (Zhang et al., 2010; Huang et al., 2011).

25 Several models to date have been developed to estimate the role of the SOA formed in the aqueous phase (denoted aqSOA hereafter). Chen et al. (2007) used a box model to investigate the formation of SOA from aqueous phase reactions in cloud water using

Global modeling of
SOA

G. Lin et al.

Title Page

Abstract

Introduction

Conclusions

References

Tables

Figures

◀

▶

◀

▶

Back

Close

Full Screen / Esc

Printer-friendly Version

Interactive Discussion



the total water mass on these seed particles, implying that SOA was formed as a result of a bulk process. On the other hand, Waxman et al. (2013) found that a surface-limited uptake process could explain the observed gas-phase glyoxal mass in Mexico City much better than a bulk phase process did. In addition, the use of an identical reactive uptake parameter for both cloud droplets and aerosol water does not account for differences in the chemistry of carbonyl compounds between cloud water and aerosol water (Lim et al., 2010; Ervens and Volkamer, 2010).

Iron chemistry in cloud water has been shown to be a major source of aqueous OH (Ervens et al., 2003; Deguillaume et al., 2005), which is known to initiate the oxidation of glyoxal and methylglyoxal in cloud water. However, no model, to our knowledge, has included the oxidation of iron in simulating the formation of aqSOA in cloud water. In addition, the amount of cloud water in a model can influence SOA production rates (Liu et al., 2012; He et al., 2013). Both issues are explored here in sensitivity tests.

In this paper, we focus on the aqueous formation of SOA from C2 and C3 carbonyl compounds not only because they are highly water soluble but also because most of the existing laboratory studies use these compounds as surrogates to examine aqueous SOA formation, so that sufficient information exists to estimate their reaction mechanisms. We use a 3-D chemical transport model to test three representations of aqueous chemistry leading to SOA formation: two detailed mechanisms using explicit multi-phase gas/aqueous phase chemical mechanisms and a parameterized surface-limited uptake mechanism using a reactive uptake parameter γ to simulate the formation of aqSOA in both cloud water and aqueous aerosol water.

This paper is organized as follows. The model and chemistry are described in Sect. 2. Global budgets and distributions of aqSOA predicted from a base mechanism are analyzed in Sect. 3. The change in global budgets of aqSOA resulting from the other four mechanisms and one different cloud field are also analyzed in Sect. 3. We compare the simulations with available measurements in Sect. 4. Finally Sect. 5 summarizes our conclusions.

2 Model description

We used the IMPACT model (Penner et al., 1998; Liu and Penner, 2002; Liu et al., 2005; Ito et al., 2007; Feng et al., 2007; Wang et al., 2009; Xu and Penner, 2012; Lin et al., 2012) to simulate the formation of SOA. The IMPACT model includes the microphysics of sulfate aerosol and the interactions between sulfate and non-sulfate aerosols based on the aerosol module developed by Herzog et al. (2004) (Liu et al., 2005). Some versions include the formation of nitrate and ammonium aerosols as well, but here, we extended the sulfate microphysics module initially described by Liu et al. (2005) to include formation on SOA (Lin et al., 2012). SOA is assumed to have a log-normal size distribution with a mode radius of $0.0774\ \mu\text{m}$ and a geometric standard deviation of 1.402. It becomes mixed with sulfate through condensation of sulfuric acid, through coagulation with pure sulfate aerosols, and through aqueous formation of sulfate. We used the 1997 meteorological fields from the National Aeronautics and Space Administration (NASA) Data Assimilation Office (DAO) GEOS-STRAT model (Coy and Swinbank, 1997; Coy et al., 1997) as input to the chemical transport model. The meteorology was defined on a 4° latitude \times 5° longitude horizontal grid with 46 vertical layers. Cloud water content was not available in our meteorological fields from the GEOS-STRAT model, and thus was diagnosed with a parameterization used in the NCAR CCM2 model (Hack, 1998); the large scale stratiform cloud fraction was determined based on the grid box mean relative humidity (RH) as calculated from the DAO meteorological data using the parameterization by Sundqvist et al. (1989). The convective cloud fraction was parameterized by using the convective mass flux (Xu and Krueger, 1991). The model was run for a 1 yr time period with a 1 month spin up time. Global emissions of gases, aerosols and aerosol precursors and treatments of dry and wet deposition used here are the same as those used in Lin et al. (2012).

2.1 SOA formation through gas-particle partitioning in the gas phase

In this paper, we adopted the gas-particle partitioning mechanism for SOA formation described by Lin et al. (2012). Lin et al. (2012) use a fully explicit gas-phase photochemical mechanism to predict the formation of semi-volatile organic compounds (SV-VOCs) which then partition to an aerosol phase. These condensed SV-VOCs were assumed to further undergo aerosol phase reactions to form oligomers with an assumed time constant (nominally 1 day). In addition, we also accounted for SOA formation due to heterogeneous reactions of epoxides on the surface of sulfate aerosol by assuming an uptake coefficient of 0.0029. Lin et al. (2012) carried out three different simulations with different gas-phase chemical mechanisms. Here, we used the most realistic mechanism ("Simulation C" in Table 1 in Lin et al., 2012). This includes the chemical mechanism published by Ito et al. (2007) to represent the basic photochemistry of O₃, OH, NO_x and VOCs, epoxide formation from isoprene from Paulot et al. (2009), and HO_x regeneration through isoprene oxidation proposed by Peeters et al. (2009) but with a reduced rate for the 1,5-H and 1,6-H shifts in isoprene radicals by a factor of 10.

2.2 SOA formation in the aqueous phase

In the presence of cloud droplets or aqueous particles, water-soluble gases (e.g., glyoxal, methylglyoxal, and glycolaldehyde) will dissolve in the aqueous phase and be further oxidized by OH and NO₃ radicals to form products with lower volatility (e.g., dicarboxylic acids and oligomers). These low volatility products are assumed to remain entirely in the particulate phase as SOA, when water is evaporated. In this paper, five aqSOA components are predicted: glyoxylic acid, pyruvic acid, oxalic acid, and two classes of oligomers formed from glyoxal and methylglyoxal.

Global modeling of SOA

G. Lin et al.

[Title Page](#)[Abstract](#)[Introduction](#)[Conclusions](#)[References](#)[Tables](#)[Figures](#)[I◀](#)[▶I](#)[◀](#)[▶](#)[Back](#)[Close](#)[Full Screen / Esc](#)[Printer-friendly Version](#)[Interactive Discussion](#)

2.2.1 Multiphase reaction scheme

The change of aqueous and gas phase species due to the photochemical reactions and the exchange between the gas and aqueous phase is expressed by the following equation,

$$\frac{dC_g}{dt} = P_g - (L_g + k_t Q) C_g + \frac{k_t}{HRT} C_a \quad (1a)$$

$$\frac{dC_a}{dt} = P_a + k_t Q C_g - (L_a + \frac{k_t}{HRT}) C_a \quad (1b)$$

Where C_a and C_g are aqueous and gas phase concentrations (molecules cm^{-3} air), P_a and P_g are aqueous and gas phase chemical production rates ($\text{mol cm}^{-3} \text{air s}^{-1}$), L_a and L_g are aqueous and gas phase pseudo-first-order chemical loss rates (s^{-1}), H is the Henry's law coefficient (M atm^{-1}), R is the universal gas constant ($\text{L atm mol}^{-1} \text{K}^{-1}$), T is the temperature (K), Q is the liquid water content ($\text{cm}^3 \text{H}_2\text{O cm}^{-3} \text{air}$), and k_t ($\text{cm}^3 \text{air cm}^{-3} \text{H}_2\text{O s}^{-1}$) is a first-order rate constant that represents diffusion through the gas phase and across the interface of the drop (see Schwartz (1986) and Lelieveld and Crutzen (1991) for details).

We used the method described by Sillman et al. (2007) to solve Eqs. (1a) and (1b). This method is based on the implicit (reverse Euler) equations but incorporates a number of nonstandard treatments as described in Sillman (1991) and Barth et al. (2003). The mass transfer rate across the gas–aqueous interface is assumed to be limited by diffusion and was determined for each gas by its molecular diffusion, mass accommodation coefficient and Henry's law constant, following methods described in Lelieveld and Crutzen (1991). A gas diffusivity of $0.1 \text{ cm}^2 \text{ s}^{-1}$ is assumed for all gaseous species. Accommodation coefficients for each species are listed in Table S7 in the Supplement and assumed to be 0.05 for species for which no information is available. For situations in which the average concentration of an aqueous species is limited by the rate

[Title Page](#)[Abstract](#)[Introduction](#)[Conclusions](#)[References](#)[Tables](#)[Figures](#)[◀](#)[▶](#)[◀](#)[▶](#)[Back](#)[Close](#)[Full Screen / Esc](#)[Printer-friendly Version](#)[Interactive Discussion](#)

Global modeling of
SOA

G. Lin et al.

Title Page

Abstract

Introduction

Conclusions

References

Tables

Figures

◀

▶

◀

▶

Back

Close

Full Screen / Esc

Printer-friendly Version

Interactive Discussion



of diffusion within the aqueous phase, the average aqueous phase concentration is scaled to the surface concentration by the factor Q as shown in Eq. (2.14) in Lelieveld and Crutzen (1991). In addition, an effective cloud droplet radius of $10\ \mu\text{m}$ is assumed for all clouds, while the effective radius for aqueous sulfate particles is calculated explicitly according to their relative humidity dependent size distributions. Aerosol water was calculated based on the water uptake by the modeled pure sulfate particles, which is based on the equilibrium Köhler theory (Ghan and Zaveri, 2007) using the RH and hygroscopicity of sulfate to calculate the wet volume mean radius from the dry volume mean radius of each mode. Water uptake by OA was not included, and thus we assume that the aerosol water associated with OA does not contribute to the formation of aqSOA. There are two reasons for this assumption. First, the reactive uptake parameter ($\gamma = 0.0029$) for glyoxal that is used for one of the mechanisms studied here was observed for wet sulfate aerosol only (Liggio et al., 2005). Second, OA is less hygroscopic than sulfate, and the uncertainty associated with neglecting the contribution of OA water is expected to be less than uncertainties caused by the observed range of reactive uptake coefficients and the photochemical reaction rate of glyoxal. Liggio et al. (2005) reported a reactive uptake coefficient for glyoxal that varied from 8.0×10^{-4} to 7.3×10^{-3} , and Ervens and Volkamer (2010) found that the derived first-order photochemical reaction rate ranges from $0.8\ \text{s}^{-1}$ to $7\ \text{s}^{-1}$ depending on the chemical composition of different seed aerosols. Finally, we ignored the formation of aqSOA in the water associated with sea salt aerosol. The terrestrial emissions of isoprene and aromatics are much larger than those from marine sources in the IMPACT model, so the aqSOA formed in the aerosol water associated with sea salt is expected to be small as well.

A complete list of aqueous phase reactions and their corresponding rate constants are given in from Tables S1 and S8 in the Supplement. Aqueous reactions for sulfates, nitrates, H_2O_2 , O_3 , OH and related radicals have been taken from Jacob (1986), Pandis and Seinfeld (1989), Lelieveld and Crutzen (1990) and Liu et al. (1997); Aqueous reactions for water-soluble organic compounds are based on recently published

box modeling studies (Lim et al., 2005; Herrmann et al., 2005; Carlton et al., 2007; Ervens and Volkamer, 2010; Lim et al., 2010); Aqueous reactions for iron are drawn from Deguillaume et al. (2010) and the Chemical Aqueous Phase Radical Mechanism (CAPRAM) 2.4 (Ervens et al., 2003).

5 While the chemistry of organic species taking place in cloud droplets is generally well established in experiments and box modeling studies, the chemistry of organic species occurring in wet particles is only now being developed so that very few models have been extended to include organic reactions (Ervens et al., 2011). Ervens and Volkamer (2010) and Lim et al. (2010) proposed different schemes for SOA formation
10 in aerosol water. Ervens and Volkamer (2010) parameterized the SOA formation using simple first order reaction rate constants to fit photochemical chamber experiments. Basically, the gas phase glyoxal is taken into aerosol water based on its Henry's law coefficient and is further hydrated to monohydrate and dihydrate glyoxal using explicit hydration coefficients for the hydration kinetics. The dissolved glyoxal, monohydrate and dihydrate glyoxals can react with dissolved OH radicals to form organic acids, or
15 undergo oligomerization using a parameterized first-order photochemical reaction rate k (unit: s^{-1}). The reactions and kinetic coefficients used in this paper are listed in Table S4 in the Supplement. The reactions in Table S4 extend the Ervens and Volkamer (2010) model for glyoxal to include the bulk phase reactions of methylglyoxal by adopting kinetic data from the literature. Lim et al. (2010) describe a second aqueous SOA
20 formation mechanism that used a set of detailed radical-radical reactions based on bulk aqueous phase experiments. Gas-phase glyoxal is partitioned into aerosol water based on its effective Henry's law constant (implicitly accounting for its hydration) and then further reacts with dissolved OH radicals to form radical species by H-atom abstraction, which combine with themselves to form dimers and trimers through so called
25 "radical-radical" reactions (Lim et al., 2010). These "radical-radical" reactions compete with reactions of the radicals with dissolved O_2 to form organic acids. In aerosol-water relevant conditions (i.e., $1\text{--}10\text{ mol L}^{-1}$ (M) glyoxal concentrations and $10^{-12}\text{--}10^{-11}$ M dissolved OH radicals), over 80 % of the products are oligomers. Since no kinetic data

Global modeling of
SOA

G. Lin et al.

Title Page

Abstract

Introduction

Conclusions

References

Tables

Figures

◀

▶

◀

▶

Back

Close

Full Screen / Esc

Printer-friendly Version

Interactive Discussion



for methylglyoxal in-aerosol-water reactions were available in Lim et al. (2010), we assumed that 80 % of products from the reaction of dissolved methylglyoxal with OH are oligomers and the rest are oxalic acid, which is consistent with the recent work of Lim et al. (2013).

5 2.2.2 Surface-limited uptake process

As an alternative to the approach described above that uses a detailed gas-phase and aqueous phase chemical mechanism coupled by gas-particle transfer, a simpler method has also been used by Fu et al. (2008) and Lin et al. (2012) to describe the uptake of a gas and its further reactions inside the particles. In this method, the loss of gas phase glyoxal or methylglyoxal on aqueous particles or cloud droplets is parameterized using the following equation:

$$\frac{dC_g}{dt} = \frac{1}{4} \cdot \gamma \cdot A \cdot \langle v \rangle \cdot C_g \quad (2)$$

Where A is the total surface area of aqueous sulfate aerosols ($\text{m}^2 \text{m}^{-3}$), C_g is the concentration of gas phase glyoxal or methylglyoxal, γ is the reactive uptake coefficient, representing the probability that a molecule impacting the particle surface undergoes reaction. The value of γ used in Fu et al. (2008) and Lin et al. (2012) was assumed to be 2.9×10^{-3} for both glyoxal and methylglyoxal uptake on aqueous sulfate and cloud droplets. $\langle v \rangle$ is the mean molecular speed of glyoxal or methylglyoxal in the gas phase given by $(8RT/\pi MW)^{-1/2}$.

20 2.3 Case set up

As described above, there are still large uncertainties in simulating aqSOA formation in both cloud water and aerosol water. We thus set up six cases to study the sensitivity of aqSOA formation to different methods representing gas-particle mass transfer and subsequent reactions (i.e., multiphase reaction scheme vs. surface-limited uptake

Title Page

Abstract

Introduction

Conclusions

References

Tables

Figures

◀

▶

◀

▶

Back

Close

Full Screen / Esc

Printer-friendly Version

Interactive Discussion



Global modeling of
SOA

G. Lin et al.

Title Page

Abstract

Introduction

Conclusions

References

Tables

Figures

◀

▶

◀

▶

Back

Close

Full Screen / Esc

Printer-friendly Version

Interactive Discussion



method), to the different chemical schemes in cloud and aerosol water reactions, to the cloud water content, and to the inclusion of iron chemistry in the cloud. The descriptions of these six cases are presented here (also summarized in Table 1), and comparisons of sensitivity test simulations with case 1 as well as with observations are shown in Sect. 3.

In case 1, we used the detailed multiphase reaction scheme (Eq. 1a, b) to predict the production of glyoxylic acid, oxalic acid and pyruvic acid in both cloud water and aerosol water (using Henry's law to predict the concentrations of glyoxal and methylglyoxal in water) and the surface-limited uptake method (Eq. 2) to predict the formation of oligomers from glyoxal and methylglyoxal. The chemical reactions of organic species used in this case are shown in Table S3 in the Supplement. Reaction rate constants were adopted from Jacob (1986), Pandis and Seinfeld (1989), Lim et al. (2005), Herrmann (2003), Herrmann et al. (2005), and Carlton et al. (2007). For simplicity, we did not consider the effect of ionic strength of cloud water on the solubility of organics, though this is expected to increase aqSOA formation (Myriokefalitakis et al., 2011). We adopted a reactive uptake coefficient γ of 3.3×10^{-3} from Waxman et al. (2013) to simulate the formation of oligomers due to glyoxal in the aerosol water. The uptake coefficient of methylglyoxal was scaled to that of glyoxal by the ratio of their effective Henry's law constants (Table S7 in the Supplement). This scaling is based on the reasoning that the glyoxal and methylglyoxal uptake by aerosol water correlates with their water solubility and that glyoxal and methylglyoxal have similar chemical reactivity and undergo similar reactions in aerosol water (Lim et al., 2013).

In case 2, all aqSOA formation was simulated using the multiphase reaction scheme. The chemical reactions in cloud water were the same as used in cloud in case 1. The parameterized reactions proposed by Ervens and Volkamer (2010) (Table S4 in the Supplement) were used for the formation of aqSOA in aerosol water replacing the chemical reaction and uptake coefficients used in case 1.

Case 3 also used the multiphase reaction scheme, but used the bulk reactions adopted from Lim et al. (2010) to predict the formation of aqSOA in both cloud and

aerosol water. The detailed bulk phase reactions of organic species used in this case are listed in Table S5 in Supplement.

For case 4, we employed the same chemical mechanism as in case 1, but used the cloud field output (in-cloud liquid water content and grid-box cloud fraction) from AM3, the atmospheric component of the coupled general circulation model (CM3) developed at the NOAA Geophysical Fluid Dynamics Laboratory (GFDL) (Donner et al., 2011) in place of the NCAR CCM2 parameterization.

In case 5, we added iron chemistry in cloud water (Table S6 in the Supplement) to the chemistry used in case 1. The only source of aqueous Fe in the model is the dissolution of dust aerosol particles incorporated into cloud droplets. We assumed that 3.5% of the mass of dust aerosol is composed of Fe (Taylor and McLennan, 1985), only 5% of which could be dissolved into cloud water (Ito and Xu, 2013). The initial speciation of Fe(II)/Fe(III) was set to 4 (Deguillaume et al., 2010).

For case 6, we used the surface-limited uptake process to simulate all aqSOA formation in both cloud and aerosol water, following the method of Fu et al. (2008) and Lin et al. (2012).

3 Results

Table 2 shows the global budget of total aqSOA and each of its components (i.e., glyoxylic acid, pyruvic acid, oxalic acid and oligomers) (if available) for these six cases. We note that the predicted oligomers in the model can consist of different numbers of monomers (e.g., dimers, trimers and tetramers), so that the total oligomers shown the cases in Table 2 do not necessarily consist of identical species. We will focus on the detailed budget and global distributions of aqSOA for case 1 in Sects. 3.1 and 3.2, and the difference between other cases with case 1 will be analyzed in Sects. 3.3 to 3.6.

Title Page

Abstract

Introduction

Conclusions

References

Tables

Figures

◀

▶

◀

▶

Back

Close

Full Screen / Esc

Printer-friendly Version

Interactive Discussion



3.1 Global budget

For case 1, the net global aqSOA production rate totals 26.7 Tgyr^{-1} , over 95 % of which is removed by wet deposition while the rest is removed by dry deposition. This rate is comparable to the SOA production rate of 29.0 Tgyr^{-1} formed from gas-particle partitioning and the rate of 25.8 Tgyr^{-1} formed from epoxide predicted in the model. The global annual mean aqSOA burden equals to 0.22 Tg , corresponding to a global mean life time of about 3.0 days due to deposition. Five aqSOA species are predicted: glyoxylic acid, pyruvic acid, oxalic acid, and two classes of oligomers formed from glyoxal and methylglyoxal. Among these five aqueous SOA components, oxalic acid accounts for about 58.8 % of total aqueous SOA source, glyoxal oligomers account for about 22.9 %, glyoxylic acid for about 16.8 %, methylglyoxal oligomers for 0.8 % and pyruvic acid for 0.7 %. While all oligomers are assumed to be formed in aerosol water, organic acids can be formed in both cloud and aerosol water. However, the contribution of aerosol water to the formation of organic acids formations is very small. The net production rate of glyoxylic acid in the aerosol water accounts for only 0.025 Tgyr^{-1} of the total 4.5 Tgyr^{-1} net production rate; 0.2 % of pyruvic acid is formed in aerosol water; for oxalic acid, the net production rate in the aerosol water (after consumption by reaction with OH) is -0.7 Tgyr^{-1} , compared to the net production rate of 16.4 Tgyr^{-1} in cloud water.

The global average reaction rates for these organic acids within cloud for case 1 are listed in Table 3. The glyoxylic acid production rate is 8.5 Tgyr^{-1} , which is derived from the oxidation of glyoxal, glycolaldehyde, methylglyoxal and acetic acid. Glyoxal oxidation accounts for 60.0 %, while the oxidation of glycolaldehyde, methylglyoxal and acetic acid account for 23.5 %, 0.8 % and 15.2 %, respectively. 47.7 % of glyoxylic acid is destroyed by reaction with OH and NO_3 , and the rest is deposited to the surface in wet deposition. For oxalic acid, the global production rate in cloud is equal to 22.7 Tgyr^{-1} , which is similar to the estimate of 21.2 Tgyr^{-1} in Simulation S1.1 (excluding the effect of ionic strength of cloud water on glyoxal, glycolaldehyde and methylglyoxal) of Myrioke-

Global modeling of SOA

G. Lin et al.

[Title Page](#)[Abstract](#)[Introduction](#)[Conclusions](#)[References](#)[Tables](#)[Figures](#)[◀](#)[▶](#)[◀](#)[▶](#)[Back](#)[Close](#)[Full Screen / Esc](#)[Printer-friendly Version](#)[Interactive Discussion](#)

Global modeling of
SOA

G. Lin et al.

Title Page

Abstract

Introduction

Conclusions

References

Tables

Figures

◀

▶

◀

▶

Back

Close

Full Screen / Esc

Printer-friendly Version

Interactive Discussion



5 falitakis et al. (2011) but larger than the estimate of 14.5 Tgyr^{-1} in Liu et al. (2012). In our model, the lumped reaction of glyoxal with OH is based on Carlton et al. (2007) and this reaction is the largest contribution (78.4%) to the total oxalic acid production; the reaction of glyoxylic acid with OH and NO_3 contributes the rest. Oxalic acid is removed from the atmosphere by OH and NO_3 radicals in aqueous phase oxidation (31.0%) and by wet and dry deposition (69.0%). The chemical destruction rate of oxalic acid is 6.3 Tgyr^{-1} . This is similar to the estimate in Simulation S1.1 of Myriokefalitakis et al. (2011) but larger than that estimated by Liu et al. (2012). Subtracting the chemical destruction rate from the production rate, the global net production rate of oxalic acid is 16.4 Tgyr^{-1} , which is comparable to the value of 13.2 Tgyr^{-1} in Simulation S1.1 of Myriokefalitakis et al. (2011) and the estimate of 13.5 Tgyr^{-1} in Liu et al. (2012). The only sources of pyruvic acid are the reactions of methylglyoxal with OH and NO_3 . In contrast to the situation for glyoxylic acid and oxalic acid, over half (73.3%) of the pyruvic acid is removed by reactions with OH and NO_3 radicals. For glyoxal and methylglyoxal oligomers, no chemical destruction is included in the model, and these are removed by wet and dry deposition.

10 The above analysis shows the importance of glyoxal, glycolaldehyde, methylglyoxal and acetic acid as precursors leading to aqueous SOA formation. The global budgets of these four species for case 1 are summarized in Table 4. While all of glyoxal, glycolaldehyde and methylglyoxal are generated by oxidation of VOCs in the gas and aqueous phase, around half of acetic acid is directly emitted into the atmosphere through biomass burning. The global glyoxal production in the gas phase is equal to 70.5 Tgyr^{-1} , while reactions in cloud water contribute 3.3 Tgyr^{-1} from the oxidation of dissolved glycolaldehyde. About 60.3% of the total glyoxal is consumed in the gas phase, while 21.3% is oxidized in cloud and 8.3% is taken up by aqueous aerosol. The rest is deposited to the surface. The total source of methylglyoxal is 167.9 Tgyr^{-1} . Of this, only 0.63 Tgyr^{-1} and 0.23 Tgyr^{-1} is absorbed and oxidized in cloud and in aqueous aerosol, respectively. Most of the methylglyoxal is destroyed in the gas phase or deposited to the surface. The net chemical production of glycolaldehyde in the gas

phase is about 17.7 Tgyr^{-1} , of which 28.8% is dissolved into cloud and reacts with OH and NO_3 . For acetic acid, the uptake rate by cloud is 0.36 Tgyr^{-1} , which can be compared to its total source strength of 60.7 Tgyr^{-1} . The uptake rate of acetic acid is smaller than the estimate of 6.96 Tgyr^{-1} by Liu et al. (2012). This is because of the smaller total atmospheric source strength of acetic acid (60.7 Tgyr^{-1} vs. 78 Tgyr^{-1}), the larger portion of gas-phase consumption of acetic acid (43% vs. 32%), and the smaller Henry's law constant ($3500 \text{ mol L}^{-1} \text{ atm}^{-1}$ vs. $8800 \text{ mol L}^{-1} \text{ atm}^{-1}$) in our model compared to those in Liu et al. (2012). Aqueous aerosol contributes a negligible amount to the sinks of both glycolaldehyde and acetic acid.

3.2 Global distribution and seasonal variability

Figure 1 presents the global annual mean surface mass concentrations (at approximately 970 hPa) of total aqSOA, total organic acids (i.e., glyoxylic acid, pyruvic acid and oxalic acid) which are mostly formed in cloud, and oligomers formed in aqueous aerosol. The zonal mean vertical distributions are also shown. The total aqSOA concentrations show large values over tropical Africa, the Amazon basin, Eastern Asia, Eastern US and Europe. The SOA distributions are determined by their precursor (mainly glyoxal) distributions, oxidant (which is primarily dissolved OH radicals) distributions, and the availability of cloud water or aerosol water. The maximum SOA concentrations over tropical Africa and the Amazon basin reflect the large biogenic VOC emissions and the resulting glyoxal concentration to a great extent. The different patterns shown for organic acid concentrations (Fig. 1c) and in oligomer concentrations (Fig. 1e) is due to the different patterns of cloud and aerosol water content (Fig. 2). Aerosol water content is due to sulfate, which spreads over the industrial regions in the Northern Hemisphere because the largest source of sulfate is from anthropogenic emissions. In contrast, most of the cloud water is located over the tropics and the Southern Hemisphere. This contrast is also reflected in the vertical zonal mean distributions of organic acids and oligomers (Fig. 1d and f). There is a hot spot in organic

[Title Page](#)[Abstract](#)[Introduction](#)[Conclusions](#)[References](#)[Tables](#)[Figures](#)[◀](#)[▶](#)[◀](#)[▶](#)[Back](#)[Close](#)[Full Screen / Esc](#)[Printer-friendly Version](#)[Interactive Discussion](#)

acids over the tropics, most of which are formed in cloud, while the peak is located over the Northern Hemisphere for the oligomers, all of which are formed in aqueous aerosols.

The column burdens of organic acids and oligomers in winter (December, January and February) and in summer (June, July, and August) are presented in Fig. 3. During the winter, the column burden of organic acids peaks over tropical land areas because of the huge biogenic emissions in these regions. During the summer, a secondary column burden maximum arises over the Northern Hemisphere land areas, which can be attributed to the enhanced photochemistry and biogenic emissions over these regions in the summer. The combination of enhanced photochemistry and larger biogenic emissions can increase the production of aqSOA precursors (e.g., glyoxal) and aqueous OH radicals, the latter due to increased H₂O₂ photolysis in cloud. For the same reason, the column burden of oligomers in the summer shows larger values that are spread over a wider area than those in the winter over the Northern Hemisphere (see the right panels in Fig. 3).

3.3 Surface-limited uptake method vs. multiphase reaction scheme

As shown in Table 2, the production rates of oligomers in case 1 are higher than those in case 2, which suggests that the value of the reactive uptake coefficient γ adopted from Waxman et al. (2013) is higher than that implied by the simulation with the detailed gas-phase and aqueous phase chemical mechanism coupled by gas-to-droplet transfer. Indeed, we can derive a global averaged γ from the Eq. (2) for the uptake of glyoxal or methglyoxal into the cloud or the aqueous aerosol from case 2. We integrated the left side and the right side of Eq. (2) globally and annually, and thus obtained the global averaged annual mean reactive uptake probability from the following equation:

$$\bar{\gamma} = \left(\sum \frac{dC_g}{dt} \right) / \left(\sum \frac{1}{4} \cdot A \cdot \langle v \rangle \cdot C_g \right) \quad (3)$$

may dominate that of the change in the aqSOA production rate. At higher altitudes (approximately between 900 hPa and 200 hPa) where the ratio of cloud water content between in case 1 and in case 4 is less than 4, the effect of the change in precursor concentrations (mainly due to the change of wet deposition rates as we show below) may dominate that of the change in the aqSOA production rate.

The lifetime of oxalic acid in case 4 is longer than that in case 1 (5.0 days in case 4 vs. 2.3 days in case 1), because in case 4 more oxalic acid is produced at high altitudes or high latitudes and less (by a factor of over 10) is formed in the low tropical regions (Fig. 4d). Oxalic acid can be precipitated out more easily in the tropics than in other regions because precipitation amounts are larger, especially that due to convective precipitation. Similarly, we have a longer lifetime of sulfate aerosol in case 4 than that in case 1. In addition, a slightly larger aqueous phase production rate of sulfate aerosol (93.3 Tgyr^{-1}) is also found in case 4 compared to that in case 1 (91.6 Tgyr^{-1}). This results from the abundant cloud water in case 4 in the Northern Hemisphere, where most of sulfate is formed. The longer lifetime and larger aqueous production rate of sulfate causes a larger sulfate burden and thus a larger oligomer formation rate in sulfate aerosol water.

3.5 The effect of iron chemistry in cloud

Inclusion of iron chemistry in cloud decreases the global average net production of aqSOA by 44% , although it increases both the chemical production and destruction of carboxylic acids in cloud (Table 2). The increase of the chemical production rate is due to the increase of the aqueous OH radical source. The global aqueous OH radical source in the troposphere (below approximately 200 hPa) in case 5 is 2.2 times larger than that in case 1 because of the formation of OH radical through the reaction of Fe(II) with H_2O_2 and the photolysis of Fe(III). The largest increase occurs over the Sahara desert, Northwestern China and Mongolia where there are large amounts of dust aerosol (Fig. 5). The enhancement of aqueous OH radicals leads to an increase of 9.3 Tgyr^{-1} in the oxalate chemical production rate and partly accounts for an increase

Global modeling of
SOA

G. Lin et al.

Title Page

Abstract

Introduction

Conclusions

References

Tables

Figures

◀

▶

◀

▶

Back

Close

Full Screen / Esc

Printer-friendly Version

Interactive Discussion



of 20.6 Tgyr^{-1} in the oxalate chemical destruction rate. Another reason for the increase in the oxalate chemical destruction rate is the fast photolysis of iron-oxalate complex $[\text{Fe}(\text{C}_2\text{O}_4)_2]^-$, which transforms $\text{C}_2\text{O}_4^{2-}$ to CO_2 . The larger increase in the chemical destruction rate compared to the chemical production rate results in a decrease in the net chemical production rate (11.3 Tgyr^{-1}), and thus a decrease in the burden as well. The inclusion of iron chemistry decreases the formation rate of glyoxal oligomers from 6.1 Tgyr^{-1} in case 1 to 5.9 Tgyr^{-1} in case 5, which is due to the increased absorption rate of glyoxal in cloud and thus less glyoxal uptake in aqueous aerosol. The absorption rate of glyoxal in cloud is increased because the increased OH radicals in cloud cause more glyoxal to be consumed in cloud so that more gas phase glyoxal can be taken up by cloud.

3.6 SOA formation in clouds vs. SOA formation in aerosol water

On a global average basis, the net SOA production rate in cloud is larger than that in aerosol water in all simulations (Table 5), although the fraction of SOA formed in cloud varies from case to case. SOA formed in cloud water accounts for about 80% of total aqSOA in case 1 and case 6; the net SOA production rate in aerosol water is even less than zero in case 2 and case 3, which means that aqSOA is consumed in aerosol water. This is because the oxalic acid formed in cloud subsequently dissolves into the aerosol water after cloud water evaporates and then further reacts with the high concentration of dissolved OH radicals inside the aerosol water, as shown in Sect. 3.1. The rate of destruction of oxalic acid by reaction with OH is larger than that of the rate of production from the reaction of glyoxalic acid and glyoxal with OH. Nevertheless, oligomers can still form in the aerosol water, with a production rate of $4.2 \times 10^{-2} \text{ Tgyr}^{-1}$ and $3.5 \times 10^{-2} \text{ Tgyr}^{-1}$ for case 2 and case 3, respectively. The amount of oligomers formed in the aerosol water is similar for cases 2 and 3 consistent with the finding by Ervens et al. (2011), who showed that their parameterized reaction system produces a similar amount of SOA as that of Lim et al. (2010) in box model simulations. The

relative importance of SOA formed in cloud water decreases to 50.3 % in case 4 when using the GFDL AM3 cloud field because of the decrease in the cloud water content in the tropics together with the increased cloud water content in the Northern Hemisphere. In case 5 with the iron chemistry in cloud, the SOA production rate in cloud explains 63.3 % of total aqSOA production rate.

4 Comparison with measurements

Figure 6 compares modeled oxalic acid with the measured oxalate compiled in Table S3 of Myriokefalitakis et al. (2011). We only show this comparison for cases 1, 4, and 5, since the oxalic acid concentrations in the other cases are similar to those in case 1 (Table 2). Although oxalate measurements are sparse around the world, the observations listed here cover most of the continentals: US, Europe, China, Amazon basin and Africa, and all these measurements have long time sampling durations which span from several days up to 2 yr . For this comparison, the monthly simulation data were sampled for the specific month and at the specific location corresponding to the measurements. It should be noted that due to the coarse resolution used in the model (4° by 5°), we don't expect the model to be able to predict the high concentrations seen in urban regions and hence we leave these out. Over rural areas, the model performance varies in different regions and different seasons. In Europe, while most of simulations in case 1 lie within a factor of 2 of the observed concentrations during the summer (see green triangles in Fig. 6), the model in case 1 underestimates all observations in winter (black dots in Fig. 6), and the discrepancy of which can be as high as an order of magnitude at some sites (e.g., K-Pustza, Hungary). The difference in the model performances between in summer and in winter may be attributed to different oxalate sources in these two seasons. According to Legrand et al. (2007), the major oxalate sources at the CARBOSOL surface stations in winter are fast secondary production in wood burning plumes and secondary production through the rapid oxidation of toluene and ethane emitted from vehicles. In summer these anthropogenic emissions decrease

Global modeling of SOA

G. Lin et al.

Title Page

Abstract

Introduction

Conclusions

References

Tables

Figures

◀

▶

◀

▶

Back

Close

Full Screen / Esc

Printer-friendly Version

Interactive Discussion



Global modeling of
SOA

G. Lin et al.

Title Page

Abstract

Introduction

Conclusions

References

Tables

Figures

◀

▶

◀

▶

Back

Close

Full Screen / Esc

Printer-friendly Version

Interactive Discussion



and biogenic emissions (e.g., isoprene) increase and make an important contribution to the oxalate source via multiphase photochemical reactions. These four CARBOSOL sites are included in the comparison here and we suspect the other European sites that we included have similar oxalate sources to those at the CARBOSOL sites. Unlike what is expected for the measurements, the model only accounts for secondary source of oxalic acid formation through multiphase photo-oxidations; the oxalic acid formation from the rapid secondary formation from local sources is not represented. Therefore the model can predict the observed oxalate concentrations relatively well in summer, whereas in winter the model under-predicts them. Other factors might also contribute to this under-estimation, such as low cloud water content or high deposition rates in the model. When using the GFDL AM3 cloud field, the model prediction improves at some sites.

As shown by the red squares in Fig. 6, the model also significantly underestimates the measured oxalate concentrations at 2 of the 3 sites in the Amazon basin. One possible reason for this underestimation is that the model does not include the oxalate source from biomass burning either through direct emission or through secondary formation from carbohydrate species in smoke aerosols (e.g., levoglucosan) during aerosol aging (Gao et al., 2003). At these two sites, biomass burning is the major source of oxalate formation (Falkovich et al., 2005; Kundu et al., 2010; Granham et al., 2002). At the site where the aerosol samples were believed to be out of the influence of biomass burning (Talbot et al., 1988), the modeled oxalate concentration in case 1 is higher than the observation, but in case 4 (using the GFDL AM3 cloud field) the model still underestimates the observation.

There are only two sites in China and three sites in US with oxalate measurements for comparison to the model. The modeled oxalate concentration is 60 % lower than the observation at the Mount Tai site reported by Wang et al. (2009), which is clean and free of local emissions. In contrast, the Mangshan site, 40 km north of Beijing, is polluted by air mass transported from Beijing (He and Kawamura, 2010), which leads to a high oxalate concentration of 760 ng m^{-3} . The model can not represent the local emissions

Global modeling of
SOA

G. Lin et al.

Title Page

Abstract

Introduction

Conclusions

References

Tables

Figures

◀

▶

◀

▶

Back

Close

Full Screen / Esc

Printer-friendly Version

Interactive Discussion



and thus only captures less than 10 % of the observation. Using the GFDL AM3 cloud field does not improve the model performance. Overestimation of oxalate deposition in the model may also contribute to this under-prediction. The three blue circles in Fig. 6 show the comparisons for the sites in US, and indicate that the model does reasonably well, except for the site in Florida Sydney. For the two sites in Africa (red stars in Fig. 6), the model fails to predict the observations. The modeled oxalate concentration in case 1 is 3 times higher than the observation at the site in Central Africa and at the site in South Africa it only predicts about 1/3 of measured concentration. This might suggest that the cloud water content in this simulation is inconsistent with the real cloud water content or that the model does not represent well the sources and/or sinks of oxalate over this region. In case 4, the model under-predicts the measurements at both of these two sites.

When including the iron chemistry in cloud in case 5, almost all of the modeled oxalate concentrations are lower than the measurements by over a factor of 2. This underestimation may be caused by an overestimation of the photolytic rate of the iron-oxalate complex and an underestimation of oxalate production rate.

Figure 6 also shows the comparison of oxalate with observations at marine sites. Most of the modeled oxalate is lower than the measurements. Myriokefalitakis et al. (2011) considered an extra glyoxal source of 20 Tgyr^{-1} over the oceans to explain the gap between the glyoxal measured from satellite and that predicted in their model. The underestimation of oxalate at marine sites in our model could also be improved by adding an extra marine source of glyoxal, although the origin of glyoxal in the marine boundary layer is still matter of debate (Rinaldi et al., 2011).

As shown above and in Sect. 3.4, cloud water has an important effect on oxalate formation. Therefore it is also valuable to compare the cloud water content in the model with that in measurements. However, there is no information available in the literature where measured oxalate concentrations were reported together with cloud water content.

Global modeling of
SOA

G. Lin et al.

Title Page

Abstract

Introduction

Conclusions

References

Tables

Figures

◀

▶

◀

▶

Back

Close

Full Screen / Esc

Printer-friendly Version

Interactive Discussion



lated the O/C ratio for each species based on their chemical formulas (see Table S1 in Lin et al., 2012). For the SOA from aerosol phase reactions of condensed SVOCs, however, it is not straightforward to calculate O/C ratio. First, we do not know the exact products from the aerosol phase reactions of condensed SVOCs, since there is very limited knowledge of these reactions in aerosol phase. Chen et al. (2011) proposed a new aerosol phase reaction for organic hydroperoxides: decomposition, followed by radical-radical oligomerization to explain the smaller measured O/C ratios than those predicted in their model. This aerosol phase reaction was shown to remove 1 ~ 2 O atoms from organic hydroperoxides. Organic nitrate is thought to undergo hydrolysis in the particle phase (Liu et al., 2012), which removes two O atoms from organic nitrate. These aerosol phase reactions proposed by Chen et al. (2011) and Liu et al. (2012) were not represented explicitly in our model. Instead, the aerosol phase reactions of condensed SVOCs were simply treated as first-order reactions to form oligomers with an assumed time constant (nominally 1 day). Despite the simple treatment for oligomer formation, we assume that the oligomers from organic hydroperoxides and organic nitrate have 1.5 O atoms and two O atoms less than condensed organic hydroperoxides and organic nitrate have, respectively, based on Chen et al. (2011) and Liu et al. (2012). For the oligomers formed from other condensed SVOCs, we assume they have the same O/C ratio as their corresponding SVOCs. An additional complexity is that in the model those 26 SOA species formed from the oligomerization of condensed SVOCs are lumped together as one species when they are transported in the atmosphere. Therefore, here we used their global-averaged SOA formation rates (listed in Table S1 in Lin et al., 2012) rather than their mass concentrations to weight their relative contributions to the O/C ratio. Based on these assumptions, we estimate the O/C ratio for the SOA from aerosol phase reactions of condensed SVOCs to be around 0.687. For SOA from the uptake of epoxide, the O/C ratio is estimated to be 0.6 since the O/C ratio of epoxide from isoprene oxidation is 0.6 in the model, and its oligomerization would not be expected to change the O/C ratio (Surratt et al., 2010). The O/C ratio for oxalic acid is 2, for glyoxylic acid is 1.5,

and for pyruvic acid is 1.0. The O/C ratio for oligomers from glyoxal and methylglyoxal is assumed to be 1.5, which is consistent with the measurements by Lim et al. (2010). We averaged the O/C ratios of these four SOA components by weighting their mass concentrations to obtain the O/C ratio for total SOA. As shown in Fig. 8, the modeled O/C ratios are higher than those reported by Ng et al. (2010) and have a normalized mean bias of 38%. The higher O/C ratios estimated in the model might suggest an overestimation of the contribution of multiple generation oxidation products to SOA formation or a missing aerosol phase reaction of condensed SVOCs that would lead to products with lower O/C ratios. Alternatively, the AMS instrument might underestimate O/C ratios.

5 Conclusions

In this paper, we simulated the formation of SOA in both cloud and aerosol water using multiphase processes with different chemical reactions and a surface-limited uptake process. We also conducted a simulation using the GFDL AM3 cloud fields and a simulation including iron chemistry in cloud. Using the surface-limited uptake process scheme with the reactive uptake parameter adopted from the laboratory studies leads to higher aqSOA production rates both in cloud and in aerosol water than using the multiphase process scheme does. Oligomers formed from glyoxal in sulfate aerosol water as predicted by the parameterized photochemistry from Ervens and Volkamer (2010) are consistent with those predicted by the detailed “radical-radical” chemistry proposed from Lim et al. (2010). The annual average organic acids (i.e. the sum of oxalic acid, glyoxylic acid, and pyruvic acid) peak over the tropical regions due to the large biogenic emissions and abundant cloud water there, while oligomers generally show maxima over industrialized areas in the Northern Hemisphere because of the large sulfate aerosol concentrations located in these regions. During the summer, however, a large organic acid concentration is also predicted in the Northern Hemisphere resulting from seasonally enhanced biogenic emissions and photochemistry. Similarly,

Title Page

Abstract

Introduction

Conclusions

References

Tables

Figures

◀

▶

◀

▶

Back

Close

Full Screen / Esc

Printer-friendly Version

Interactive Discussion



Global modeling of
SOA

G. Lin et al.

Title Page

Abstract

Introduction

Conclusions

References

Tables

Figures

I◀

▶I

◀

▶

Back

Close

Full Screen / Esc

Printer-friendly Version

Interactive Discussion



the oligomer concentrations increase in the summer. When we changed the diagnostic cloud field to that simulated by the GFDL AM3 model, the organic acid production rate decreased by around 60 % while sulfate formation rates increased slightly, because the GFDL AM3 cloud field has a much smaller cloud water content in tropical regions but a higher cloud water content in the Northern Hemisphere. The aqSOA formation rate in cloud water is about equal to that in aerosol water in the simulation with the GFDL AM3 cloud field, while in the other simulations with the diagnostic cloud field the aqSOA formation rate in cloud water dominate over that in aerosol water. The introduction of Fe chemistry in cloud has a large impact on the aqueous phase HO_x and aqSOA budget, increasing the global average tropical aqueous OH radical source by a factor of about 2.2 and decreasing the net source of aqSOA by 44 %.

We also compared the oxalic acid predicted from these different schemes and chemical mechanisms with measurements obtained in Europe, Amazon, Africa, China and US region. Over all, the model without considering the iron chemistry in cloud tends to underestimate observations in Europe in winter, as well as in Amazon, Africa, and China, probably because the model does not account for the direct emission of oxalic acid from primary sources (e.g., wood burning, meat cooking and biomass burning) or the oxalic acid formed in the aging process associated with these direct emissions. However, this underestimation might also be due to a deposition rate that is too high or a cloud water content that is too low in the model. In fact, using the GFDL AM3 cloud field in case 4 improved the model predictions at some sites in the Northern Hemisphere. Further comparisons are needed in the future when both the cloud water content and aqSOA in cloud are available. Consistent with the findings of Myriokefalitakis et al. (2011), the comparison of oxalate for marine sites suggests that there may be a missing source of oxalic acid over the ocean in the model. When including the iron chemistry in cloud, the model under-predicts nearly all of the measured concentrations of oxalate by over a factor of 2. This underestimation indicates that further study is needed to understand the oxalate formation well.

Global modeling of
SOA

G. Lin et al.

Title Page

Abstract

Introduction

Conclusions

References

Tables

Figures

I◀

▶I

◀

▶

Back

Close

Full Screen / Esc

Printer-friendly Version

Interactive Discussion



Comparisons of the total SOA (aqSOA combined with the SOA formed in the gas phase) for all cases with the SOA measured by AMS in the Northern Hemisphere show reasonable agreement, although the NMB varies between +20 % in case 6 (which used a surface-based uptake coefficient method for aqSOA both in cloud and aerosol water) to around –40 % in Cases 2 and 3 (which used a complete or a parameterized multi-phase reaction scheme for aqSOA). While case 6 over-estimates the observations by a factor of over 3 at West Africa site and a factor of over 2 at the other two tropical sites, adopting the multiphase reaction scheme for aqSOA decrease the disagreement to within a factor of 2 at all three sites. In addition to the SOA mass measured by AMS, we compared the O/C ratio of OOA estimated based on a factor analysis of AMS measurements to the O/C ratio of modeled SOA based on some simple assumptions. The estimated O/C ratios from the model are somewhat higher than those estimated from the measurements, which might indicate that the model overestimates the contribution of aged organic species to SOA formation.

Supplementary material related to this article is available online at <http://www.atmos-chem-phys-discuss.net/13/29629/2013/acpd-13-29629-2013-supplement.pdf>.

Acknowledgements. The authors are grateful for support by the Department of Energy (DOE) Earth System Modeling program through grant number DOE FG02 01 ER63248, support from the DOE Atmospheric Science Research Program through grant number DoE DE-SC0008486, and support from EPA Science to Achieve Results (STAR) program, grant #R-83337701. A. Ito's work at JAMSTEC was supported under Program for Risk Information on Climate Change by MEXT.

References

- Aiken, A. C., DeCarlo, P. F., Kroll, J. H., Worsnop, D. R., Huffman, J. A., Docherty, K. S., Ulbrich, I. M., Mohr, C., Kimmel, J. R., Sueper, D., Sun, Y., Zhang, Q., Trimborn, A., Northway, M., Ziemann, P. J., Canagaratna, M. R., Onasch, T. B., Alfarra, M. R., Prevot, A. S. H., Dommen, J., Duplissy, J., Metzger, A., Baltensperger, U., and Jimenez, J. L.: O/C and OM/OC ratios of primary, secondary, and ambient organic aerosols with high-resolution time-of-flight aerosol mass spectrometry, *Environ. Sci. Technol.*, 42, 4478–4485, doi:10.1021/es703009q, 2008.
- Altieri, K. E., Seitzinger, S. P., Carlton, A. G., Turpin, B. J., Klein, G. C., and Marshall, A. G.: Oligomers formed through in-cloud methylglyoxal reactions: chemical composition, properties, and mechanisms investigated by ultra-high resolution FT-ICR mass spectrometry, *Atmos. Environ.*, 42, 1476–1490, doi:10.1016/j.atmosenv.2007.11.015, 2008.
- Altieri, K. E., Turpin, B. J., and Seitzinger, S. P.: Composition of dissolved organic nitrogen in continental precipitation investigated by ultra-high resolution FT-ICR mass spectrometry, *Environ. Sci. Technol.*, 43, 6950–6955, doi:10.1021/es9007849, 2009.
- Barth, M. C., Sillman, S., Hudman, R., Jacobson, M. Z., Kim, C. H., Monod, A., and Liang, J.: Summary of the cloud chemistry modeling intercomparison: photochemical box model simulation, *J. Geophys. Res.-Atmos.*, 108, 4214, doi:10.1029/2002JD002673, 2003.
- Blando, J. D. and Turpin, B. J.: Secondary organic aerosol formation in cloud and fog droplets: a literature evaluation of plausibility, *Atmos. Environ.*, 34, 1623–1632, 2000.
- Capes, G., Murphy, J. G., Reeves, C. E., McQuaid, J. B., Hamilton, J. F., Hopkins, J. R., Crosier, J., Williams, P. I., and Coe, H.: Secondary organic aerosol from biogenic VOCs over West Africa during AMMA, *Atmos. Chem. Phys.*, 9, 3841–3850, doi:10.5194/acp-9-3841-2009, 2009.
- Carlton, A. G., Turpin, B. J., Lim, H. J., Altieri, K. E., and Seitzinger, S.: Link between isoprene and secondary organic aerosol (SOA): pyruvic acid oxidation yields low volatility organic acids in clouds, *Geophys. Res. Lett.*, 33, L06822, doi:10.1029/2005GL025374, 2006.
- Carlton, A. G., Turpin, B. J., Altieri, K. E., Seitzinger, S., Reff, A., Lim, H. J., and Ervens, B.: Atmospheric oxalic acid and SOA production from glyoxal: results of aqueous photooxidation experiments, *Atmos. Environ.*, 41, 7588–7602, doi:10.1016/j.atmosenv.2007.05.035, 2007.
- Carlton, A. G., Turpin, B. J., Altieri, K. E., Seitzinger, S. P., Mathur, R., Roselle, S. J., and Weber, R. J.: CMAQ model performance enhanced when in-cloud secondary organic aerosol

Global modeling of SOA

G. Lin et al.

Title Page

Abstract

Introduction

Conclusions

References

Tables

Figures

◀

▶

◀

▶

Back

Close

Full Screen / Esc

Printer-friendly Version

Interactive Discussion



Global modeling of
SOA

G. Lin et al.

Title Page

Abstract

Introduction

Conclusions

References

Tables

Figures

◀

▶

◀

▶

Back

Close

Full Screen / Esc

Printer-friendly Version

Interactive Discussion



is included: comparisons of organic carbon predictions with measurements, Environ. Sci. Technol., 42, 8789–8802, 2008.

Chen, J., Griffin, R. J., Grini, A., and Tulet, P.: Modeling secondary organic aerosol formation through cloud processing of organic compounds, Atmos. Chem. Phys., 7, 5343–5355, doi:10.5194/acp-7-5343-2007, 2007.

Chen, Q., Farmer, D. K., Schneider, J., Zorn, S. R., Heald, C. L., Karl, T. G., Guenther, A., Allan, J. D., Robinson, N., Coe, H., Kimmel, J. R., Pauliquevis, T., Borrmann, S., Pöschl, U., Andreae, M. O., Artaxo, P., Jimenez, J. L., and Martin, S. T.: Mass spectral characterization of submicron biogenic organic particles in the Amazon Basin, Geophys. Res. Lett., 36, L20806, doi:10.1029/2009gl039880, 2009.

Chen, Q., Liu, Y., Donahue, N. M., Shilling, J. E., and Martin, S. T.: Particle-phase chemistry of secondary organic material: modeled compared to measured O : C and H : C elemental ratios provide constraints, Environ. Sci. Technol., 45, 4763–4770, doi:10.1021/es104398s, 2011.

Coy, L. and Swinbank, R.: Characteristics of stratospheric winds and temperatures produced by data assimilation, J. Geophys. Res., 102, 25763–25781, 1997.

Coy, L., Nash, E. R., and Newman, P. A.: Meteorology of the polar vortex: spring 1997, Geophys. Res. Lett., 24, 2693–2696, 1997.

DeGouw, J. A., Middlebrook, A. M., Warneke, C., Goldan, P. D., Kuster, W. C., Roberts, J. M., Fehsenfeld, F. C., Worsnop, D. R., Canagaratna, M. R., Pszenny, A. A. P., Keene, W. C., Marchewka, M., Bertram, S. B., and Bates, T. S.: Budget of organic carbon in a polluted atmosphere: results from the New England Air Quality Study in 2002, J. Geophys. Res., 110, D16305, doi:10.1029/2004JD005623, 2005.

Deguillaume, L., Leriche, M., and Desboeufs, K.: Transition metals in atmospheric liquid phases: sources, reactivity, and sensitive parameters, Chem. Rev., 105, 3388–3431, 2005.

Deguillaume, L., Desboeufs, K. V., Leriche, M., Long, Y., and Chaumerliac, N.: Effect of iron dissolution on cloud chemistry: from laboratory measurements to model results, Atmos. Pollut. Res., 1, 220–228, 2010.

Donner, L. J., Wyman, B. L., Hemler, R. S., Horowitz, L. W., Ming, Y., Zhao, M., Golaz, J.-C., Ginoux, P., Lin, S. J., Schwarzkopf, D. M., Austin, J., Alaka, G., Cooke, W. F., Delworth, T. L., Freidenreich, S. M., Gordon, C. T., Grif?es, S. M., Held, I. M., Hurlin, W. J., Klein, S. A., Knutson, T. R., Langenhorst, A. R., Lee, H.-C., Lin, Y., Magi, B. I., Malyshev, S. L., Milly, P. C. D., Naik, V., Nath, M. J., Pincus, R., Ploshay, J. J., Ramaswamy, V., Seman,

Global modeling of
SOA

G. Lin et al.

Title Page

Abstract

Introduction

Conclusions

References

Tables

Figures

◀

▶

◀

▶

Back

Close

Full Screen / Esc

Printer-friendly Version

Interactive Discussion



C. J., Shevliakova, E., Sirutis, J. J., Stern, W. F., Stouffer, R. J., Wilson, R. J., Winton, M., Wittenberg, A. T., and Zeng, F.: The dynamical core, physical parameterizations, and basic simulation characteristics of the atmospheric component AM3 of the GFDL global coupled model CM3, *J. Climate*, 24, 3484–3519, doi:10.1175/2011JCLI3955.1, 2011.

5 Dzepina, K., Volkamer, R. M., Madronich, S., Tulet, P., Ulbrich, I. M., Zhang, Q., Cappa, C. D., Ziemann, P. J., and Jimenez, J. L.: Evaluation of recently-proposed secondary organic aerosol models for a case study in Mexico City, *Atmos. Chem. Phys.*, 9, 5681–5709, doi:10.5194/acp-9-5681-2009, 2009.

10 El Haddad, I., Yao Liu, Nieto-Gligorovski, L., Michaud, V., Temime-Roussel, B., Quivet, E., Marchand, N., Sellegri, K., and Monod, A.: In-cloud processes of methacrolein under simulated conditions – Part 2: Formation of secondary organic aerosol, *Atmos. Chem. Phys.*, 9, 5107–5117, doi:10.5194/acp-9-5107-2009, 2009.

Eliason, T. L., Aloisio, S., Donaldson, D. J., Cziczo, D. J., and Vaida, V.: Processing of unsaturated organic acid films and aerosols by ozone, *Atmos. Environ.*, 37, 2207–2219, doi:10.1016/S1352-2310(03)00149-3, 2003.

15 Ervens, B. and Volkamer, R.: Glyoxal processing by aerosol multiphase chemistry: towards a kinetic modeling framework of secondary organic aerosol formation in aqueous particles, *Atmos. Chem. Phys.*, 10, 8219–8244, doi:10.5194/acp-10-8219-2010, 2010.

20 Ervens, B., George, C., Williams, J. E., Buxton, G. V., Salmon, G. A., Bydder, M., Wilkinson, F., Dentener, F., Mirabel, P., Wolke, R., and Herrmann, H.: CAPRAM 2.4 (MODAC mechanism): an extended and condensed tropospheric aqueous phase mechanism and its application, *J. Geophys. Res.*, 108, 4426, doi:10.1029/2002JD002202, 2003.

25 Ervens, B., Carlton, A. G., Turpin, B. J., Altieri, K. E., Kreidenweis, S. M., and Feingold, G.: Secondary organic aerosol yields from cloud processing of isoprene oxidation products, *Geophys. Res. Lett.*, 35, L02816, doi:10.1029/2007gl031828, 2008.

Ervens, B., Turpin, B. J., and Weber, R. J.: Secondary organic aerosol formation in cloud droplets and aqueous particles (aqSOA): a review of laboratory, field and model studies, *Atmos. Chem. Phys.*, 11, 11069–11102, doi:10.5194/acp-11-11069-2011, 2011.

30 Falkovich, A. H., Graber, E. R., Schkolnik, G., Rudich, Y., Maenhaut, W., and Artaxo, P.: Low molecular weight organic acids in aerosol particles from Rondônia, Brazil, during the biomass-burning, transition and wet periods, *Atmos. Chem. Phys.*, 5, 781–797, doi:10.5194/acp-5-781-2005, 2005.

Global modeling of
SOA

G. Lin et al.

Title Page

Abstract

Introduction

Conclusions

References

Tables

Figures

◀

▶

◀

▶

Back

Close

Full Screen / Esc

Printer-friendly Version

Interactive Discussion



- Feng, Y. and Penner, J. E.: Global modeling of nitrate and ammonium: Interaction of aerosols and tropospheric chemistry, *J. Geophys. Res.*, 112, D01304, doi:10.1029/2005JD006404, 2007.
- 5 Fu, T. M., Jacob, D. J., Wittrock, F., Burrows, J. P., Vrekoussis, M., and Henze, D. K.: Global budgets of atmospheric glyoxal and methylglyoxal, and implications for formation of secondary organic aerosols, *J. Geophys. Res.*, 113, D15303, doi:10.1029/2007jd009505, 2008.
- Fu, T. M., Jacob, D. J., and Heald, C. L.: Aqueous-phase reactive uptake of dicarbonyls as a source of organic aerosol over eastern North America, *Atmos. Environ.*, 43, 1814–1822, 2009.
- 10 Gao, S., Hegg, D. A., Hobbs, P. V., Kirchstetter, T. W., Magi, B. I., and Sadilek, M.: Water-soluble organic components in aerosols associated with savanna fires in Southern Africa: identification, evolution, and distribution, *J. Geophys. Res.*, 108, 8491, doi:10.1029/2002JD002324, 2003.
- Ghan, S. J. and Zaveri, R. A.: Parameterization of optical properties for hydrated internally mixed aerosol, *J. Geophys. Res.*, 112, D10201, doi:10.1029/2006JD007927, 2007.
- 15 Gilardoni, S., Vignati, E., Marmer, E., Cavalli, F., Belis, C., Gianelle, V., Loureiro, A., and Artaxo, P.: Sources of carbonaceous aerosol in the Amazon basin, *Atmos. Chem. Phys.*, 11, 2747–2764, doi:10.5194/acp-11-2747-2011, 2011.
- Graham, B., Mayol-Bracero, O. L., Guyon, P., Roberts, G. C., Decesari, S., Facchini, M. C., Artaxo, P., Maenhaut, W., Koll, P., and Andreae, M. O.: Water-soluble organic compounds in biomass burning aerosols over Amazonia, characterization by NMR and GC-MS, *J. Geophys. Res.*, 107, 8047, doi:10.1029/2001JD000336, 2002.
- 20 Hack, J. J.: Sensitivity of the simulated climate to a diagnostic formulation for cloud liquid water, *J. Climate*, 11, 1497–1515, 1998.
- 25 He, C., Liu, J., Carlton, A. G., Fan, S., Horowitz, L. W., Levy II, H., and Tao, S.: Evaluation of factors controlling global secondary organic aerosol production from cloud processes, *Atmos. Chem. Phys.*, 13, 1913–1926, doi:10.5194/acp-13-1913-2013, 2013.
- He, N. and Kawamura, K.: Distributions and diurnal changes of low molecular weight organic acids and α -dicarbonyls in suburban aerosols collected at Mangshan, North China, *Geochem. J.*, 44, e17–e22, 2010.
- 30 Heald, C. L., Jacob, D. J., Park, R. J., Russell, L. M., Huebert, B. J., Seinfeld, J. H., Liao, H., and Weber, R. J.: A large organic aerosol source in the free troposphere missing from current models, *Geophys. Res. Lett.*, 32, L18809, doi:10.1029/2005GL023831, 2005.

Global modeling of
SOA

G. Lin et al.

Title Page

Abstract

Introduction

Conclusions

References

Tables

Figures

◀

▶

◀

▶

Back

Close

Full Screen / Esc

Printer-friendly Version

Interactive Discussion



- Herrmann, H.: Kinetics of aqueous phase reactions relevant for atmospheric chemistry, *Chem. Rev.*, 103, 4691–4716, 2003.
- Herrmann, H., Tilgner, A., Barzagli, P., Majdik, Z., Gligorovski, S., Poulain, L., and Monod, A.: Towards a more detailed description of tropospheric aqueous phase organic chemistry: CAPRAM 3.0, *Atmos. Environ.*, 39, 4351–4363, doi:10.1016/j.atmosenv.2005.02.016, 2005.
- Herzog, M., Weisenstein, D. K., and Penner, J. E.: A dynamic aerosol module for global chemical transport models: model description, *J. Geophys. Res.*, 109, D18202, doi:10.1029/2003jd004405, 2004.
- Hodzic, A., Jimenez, J. L., Madronich, S., Canagaratna, M. R., DeCarlo, P. F., Kleinman, L., and Fast, J.: Modeling organic aerosols in a megacity: potential contribution of semi-volatile and intermediate volatility primary organic compounds to secondary organic aerosol formation, *Atmos. Chem. Phys.*, 10, 5491–5514, doi:10.5194/acp-10-5491-2010, 2010.
- Huang, D., Zhang, X., Chen, Z. M., Zhao, Y., and Shen, X. L.: The kinetics and mechanism of an aqueous phase isoprene reaction with hydroxyl radical, *Atmos. Chem. Phys.*, 11, 7399–7415, doi:10.5194/acp-11-7399-2011, 2011.
- Ito, A. and Xu, L.: Response of acid mobilization of iron-containing mineral dust to improvement of air quality projected in the future, *Atmos. Chem. Phys. Discuss.*, 13, 28173–28223, doi:10.5194/acpd-13-28173-2013, 2013.
- Ito, A., Sillman, S., and Penner, J. E.: Effects of additional nonmethane volatile organic compounds, organic nitrates, and direct emissions of oxygenated organic species on global tropospheric chemistry, *J. Geophys. Res.*, 112, D06309, doi:10.1029/2005jd006556, 2007.
- Jacob, D. J.: Chemistry of OH in remote clouds and its role in the production of formic acid and peroxymonosulfate, *J. Geophys. Res.*, 91, 9807–9826, doi:10.1029/JD091iD09p09807, 1986.
- Jimenez, J. L., Canagaratna, M. R., Donahue, N. M., Prevot, A. S. H., Zhang, Q., Kroll, J. H., DeCarlo, P. F., Allan, J. D., Coe, H., Ng, N. L., Aiken, A. C., Docherty, K. S., Ulbrich, I. M., Grieshop, A. P., Robinson, A. L., Duplissy, J., Smith, J. D., Wilson, K. R., Lanz, V. A., Hueglin, C., Sun, Y. L., Tian, J., Laaksonen, A., Raatikainen, T., Rautiainen, J., Vaattovaara, P., Ehn, M., Kulmala, M., Tomlinson, J. M., Collins, D. R., Cubison, M. J., Dunlea, E. J., Huffman, J. A., Onasch, T. B., Alfarra, M. R., Williams, P. I., Bower, K., Kondo, Y., Schneider, J., Drewnick, F., Borrmann, S., Weimer, S., Demerjian, K., Salcedo, D., Cottrell, L., Griffin, R., Takami, A., Miyoshi, T., Hatakeyama, S., Shimono, A., Sun, J. Y., Zhang, Y. M., Dzepina, K., Kimmel, J. R., Sueper, D., Jayne, J. T., Herndon, S. C., Trimborn, A. M., Williams, L. R., Wood, E. C.,

Global modeling of
SOA

G. Lin et al.

Title Page

Abstract

Introduction

Conclusions

References

Tables

Figures

◀

▶

◀

▶

Back

Close

Full Screen / Esc

Printer-friendly Version

Interactive Discussion



- Middlebrook, A. M., Kolb, C. E., Baltensperger, U., and Worsnop, D. R.: Evolution of organic aerosols in the atmosphere, *Science*, 326, 1525–1529, doi:10.1126/science.1180353, 2009.
- Kundu, S., Kawamura, K., Lee, M., Andreae, T. W., Hoffer, A., and Andreae, M. O.: Comparison of Amazonian biomass burning and East Asian marine aerosols: bulk organics, diacids and related compounds, water-soluble inorganic ions, stable carbon and nitrogen isotope ratios, *Low Temp. Sci.*, 68, 89–100, 2010.
- Lee-Taylor, J., Madronich, S., Aumont, B., Baker, A., Camredon, M., Hodzic, A., Tyndall, G. S., Apel, E., and Zaveri, R. A.: Explicit modeling of organic chemistry and secondary organic aerosol partitioning for Mexico City and its outflow plume, *Atmos. Chem. Phys.*, 11, 13219–13241, doi:10.5194/acp-11-13219-2011, 2011.
- Legrand, M., Preunkert, S., Oliveira, T., Pio, C. A., Hammer, S., Gelencsér, A., Kasper-Giebl, A., and Laj, P.: Origin of C₂–C₅ dicarboxylic acids in the European atmosphere inferred from year-round aerosol study conducted at a west-east transect, *J. Geophys. Res.*, 112, D23S07, doi:10.1029/2006JD008019, 2007.
- Lelieveld, J. and Crutzen, P. J.: The role of clouds in tropospheric photochemistry, *J. Atmos. Chem.*, 12, 229–267, doi:10.1007/BF00048075, 1991.
- Liggio, J., Li, S. M., and McLaren, R.: Heterogeneous reactions of glyoxal on particulate matter: identification of acetals and sulfate esters, *Environ. Sci. Technol.*, 39, 1532–1541, 2005.
- Lim, H. J., Carlton, A. G., and Turpin, B. J.: Isoprene forms secondary organic aerosol through cloud processing: model simulations, *Environ. Sci. Technol.*, 9, 4441–4446, 2005.
- Lim, Y. B., Tan, Y., Perri, M. J., Seitzinger, S. P., and Turpin, B. J.: Aqueous chemistry and its role in secondary organic aerosol (SOA) formation, *Atmos. Chem. Phys.*, 10, 10521–10539, doi:10.5194/acp-10-10521-2010, 2010.
- Lim, Y. B., Tan, Y., and Turpin, B. J.: Chemical insights, explicit chemistry, and yields of secondary organic aerosol from OH radical oxidation of methylglyoxal and glyoxal in the aqueous phase, *Atmos. Chem. Phys.*, 13, 8651–8667, doi:10.5194/acp-13-8651-2013, 2013.
- Lin, G., Penner, J. E., Sillman, S., Taraborrelli, D., and Lelieveld, J.: Global modeling of SOA formation from dicarbonyls, epoxides, organic nitrates and peroxides, *Atmos. Chem. Phys.*, 12, 4743–4774, doi:10.5194/acp-12-4743-2012, 2012.
- Liu, J., Horowitz, L. W., Fan, S., Carlton, A. G., and Levy II, H.: Global in-cloud production of secondary organic aerosols: implementation of a detailed chemical mechanism in the GFDL atmospheric model AM3, *J. Geophys. Res.*, 117, D15303, doi:10.1029/2012JD017838, 2012.

Global modeling of
SOA

G. Lin et al.

Title Page

Abstract

Introduction

Conclusions

References

Tables

Figures

◀

▶

◀

▶

Back

Close

Full Screen / Esc

Printer-friendly Version

Interactive Discussion



- Liu, S., Shilling, J. E., Song, C., Hiranuma, N., Zaveri, R. A., and Russell, L. M.: Hydrolysis of organonitrate functional groups in aerosol particles, *Aerosol Sci. Tech.*, 46, 1359–1369, 2012.
- Liu, X. H. and Penner, J. E.: Effect of Mount Pinatubo $\text{H}_2\text{SO}_4/\text{H}_2\text{O}$ aerosol on ice nucleation in the upper troposphere using a global chemistry and transport model, *J. Geophys. Res.*, 107, 4141–4157, doi:10.1029/2001JD000455, 2002.
- Liu, X. H., Penner, J. E., and Herzog, M.: Global modeling of aerosol dynamics: Model description, evaluation, and interactions between sulfate and nonsulfate aerosols, *J. Geophys. Res.*, 110, D18206, doi:10.1029/2004jd005674, 2005.
- Liu, X., Mauersberger, G., and Möller, D.: The effects of cloud processes on the tropospheric photochemistry: an improvement of the eurad model with a coupled gaseous and aqueous chemical mechanism, *Atmos. Environ.*, 31, 3119–3135, doi:10.1016/S1352-2310(97)00057-5, 1997.
- Myriokefalitakis, S., Tsigaridis, K., Mihalopoulos, N., Sciare, J., Nenes, A., Kawamura, K., Segers, A., and Kanakidou, M.: In-cloud oxalate formation in the global troposphere: a 3-D modeling study, *Atmos. Chem. Phys.*, 11, 5761–5782, doi:10.5194/acp-11-5761-2011, 2011.
- Ng, N. L., Chhabra, P. S., Chan, A. W. H., Surratt, J. D., Kroll, J. H., Kwan, A. J., McCabe, D. C., Wennberg, P. O., Sorooshian, A., Murphy, S. M., Dalleska, N. F., Flagan, R. C., and Seinfeld, J. H.: Effect of NO_x level on secondary organic aerosol (SOA) formation from the photooxidation of terpenes, *Atmos. Chem. Phys.*, 7, 5159–5174, doi:10.5194/acp-7-5159-2007, 2007.
- Ng, N. L., Canagaratna, M. R., Zhang, Q., Jimenez, J. L., Tian, J., Ulbrich, I. M., Kroll, J. H., Docherty, K. S., Chhabra, P. S., Bahreini, R., Murphy, S. M., Seinfeld, J. H., Hildebrandt, L., Donahue, N. M., DeCarlo, P. F., Lanz, V. A., Prévôt, A. S. H., Dinar, E., Rudich, Y., and Worsnop, D. R.: Organic aerosol components observed in Northern Hemispheric datasets from Aerosol Mass Spectrometry, *Atmos. Chem. Phys.*, 10, 4625–4641, doi:10.5194/acp-10-4625-2010, 2010.
- Odum, J. R., Hoffmann, T., Bowman, F., Collins, D., Flagan, R. C., and Seinfeld, J. H.: Gas/particle partitioning and secondary organic aerosol yields, *Environ. Sci. Technol.*, 30, 2580–2585, 1996.
- Pandis, S. N. and Seinfeld, J. H.: Sensitivity analysis of a chemical mechanism for aqueous-phase atmospheric chemistry, *J. Geophys. Res.*, 94, 1105–1126, doi:10.1029/JD094iD01p01105, 1989.

Global modeling of
SOA

G. Lin et al.

Title Page

Abstract

Introduction

Conclusions

References

Tables

Figures

◀

▶

◀

▶

Back

Close

Full Screen / Esc

Printer-friendly Version

Interactive Discussion



- Pankow, J. F.: An absorption model of gas/particle partitioning of organic compounds in the atmosphere, *Atmos. Environ.*, 28, 185–188, doi:10.1016/1352-2310(94)90093-0, 1994.
- Paulot, F., Crounse, J. D., Kjaergaard, H. G., Kurten, A., St Clair, J. M., Seinfeld, J. H., and Wennberg, P. O.: Unexpected epoxide formation in the gas-phase photooxidation of isoprene, *Science*, 325, 730–733, doi:10.1126/science.1172910, 2009.
- Peeters, J., Nguyen, T. L., and Vereecken, L.: HO_x radical regeneration in the oxidation of isoprene, *Phys. Chem. Chem. Phys.*, 11, 5935–5939, doi:10.1039/b908511d, 2009.
- Penner, J. E., Chuang, C. C., and Grant, K.: Climate forcing by carbonaceous and sulfate aerosols, *Clim. Dynam.*, 14, 839–851, 1998.
- Perri, M. J., Seitzinger, S., and Turpin, B. J.: Secondary organic aerosol production from aqueous photooxidation of glycolaldehyde: laboratory experiments, *Atmos. Environ.*, 43, 1487–1497, 2009.
- Pye, H. O. T. and Seinfeld, J. H.: A global perspective on aerosol from low-volatility organic compounds, *Atmos. Chem. Phys.*, 10, 4377–4401, doi:10.5194/acp-10-4377-2010, 2010.
- Rinaldi, M., Decesari, S., Carbone, C., Finessi, E., Fuzzi, S., Ceburnis, D., O'Dowd, C., Sciare, J., Burrows, J., Vrekoussis, M., Ervens, B., Tsigaridis, K., and Fachini, M. C.: Evidence of a natural marine source of oxalic acid and a possible link to glyoxal, *J. Geophys. Res.*, 116, D16204, doi:10.1029/2011JD015659, 2011.
- Robinson, A. L., Donahue, N. M., Shrivastava, M. K., Weitkamp, E. A., Sage, A. M., Grieshop, A. P., Lane, T. E., Pierce, J. R., and Pandis, S. N.: Rethinking organic aerosols: semivolatile emissions and photochemical aging, *Science*, 315, 1259–1262, doi:10.1126/science.1133061, 2007.
- Robinson, N. H., Hamilton, J. F., Allan, J. D., Langford, B., Oram, D. E., Chen, Q., Docherty, K., Farmer, D. K., Jimenez, J. L., Ward, M. W., Hewitt, C. N., Barley, M. H., Jenkin, M. E., Rickard, A. R., Martin, S. T., McFiggans, G., and Coe, H.: Evidence for a significant proportion of Secondary Organic Aerosol from isoprene above a maritime tropical forest, *Atmos. Chem. Phys.*, 11, 1039–1050, doi:10.5194/acp-11-1039-2011, 2011.
- Schwartz, S. E.: Mass-transport considerations pertinent to aqueous phase reactions of gases on liquid water clouds, in: *Chemistry of Multiphase Atmospheric Systems*, NATO ASI Ser., edited by: Jaeschke, W., Springer, Berlin, Germany, 1986.
- Sillman, S.: A numerical-solution for the equations of tropospheric chemistry based on an analysis of sources and sinks of odd hydrogen, *J. Geophys. Res.*, 96, 20735–20744, 1991.

Global modeling of
SOA

G. Lin et al.

Title Page

Abstract

Introduction

Conclusions

References

Tables

Figures

◀

▶

◀

▶

Back

Close

Full Screen / Esc

Printer-friendly Version

Interactive Discussion



- Sillman, S., Marsik, F. J., Al-Wali, K. I., Keeler, G. J., and Landis, M. S.: Reactive mercury in the troposphere: model formation and results for Florida, the Northeastern US, and the Atlantic Ocean, *J. Geophys. Res.*, 112, D23305, doi:10.1029/2006JD008227, 2007.
- 5 Sorooshian, A., Lu, M. L., Brechtel, F. J., Jonsson, H., Feingold, G., Flagan, R. C., and Seinfeld, J. H.: On the source of organic acid aerosol layers above clouds, *Environ. Sci. Technol.*, 41, 4647–4654, 2007.
- Spracklen, D. V., Jimenez, J. L., Carslaw, K. S., Worsnop, D. R., Evans, M. J., Mann, G. W., Zhang, Q., Canagaratna, M. R., Allan, J., Coe, H., McFiggans, G., Rap, A., and Forster, P.: Aerosol mass spectrometer constraint on the global secondary organic aerosol budget, *Atmos. Chem. Phys.*, 11, 12109–12136, doi:10.5194/acp-11-12109-2011, 2011.
- 10 Stavrakou, T., Müller, J.-F., De Smedt, I., Van Roozendael, M., Kanakidou, M., Vrekoussis, M., Wittrock, F., Richter, A., and Burrows, J. P.: The continental source of glyoxal estimated by the synergistic use of spaceborne measurements and inverse modelling, *Atmos. Chem. Phys.*, 9, 8431–8446, doi:10.5194/acp-9-8431-2009, 2009.
- 15 Sundqvist, H., Berge, E., and Kristjánsson, J. E.: Condensation and cloud parameterization studies with a mesoscale numerical weather prediction model, *Mon. Weather Rev.*, 117, 1641–1657, 1989.
- Surratt, J. D., Chan, A. W. H., Eddingsaas, N. C., Chan, M. N., Loza, C. L., Kwan, A. J., Hersey, S. P., Flagan, R. C., Wennberg, P. O., and Seinfeld, J. H.: Reactive intermediates revealed in secondary organic aerosol formation from isoprene, *P. Natl. Acad. Sci. USA*, 20 107, 6640–6645, doi:10.1073/pnas.0911114107, 2010.
- Talbot, R. W., Andreae, M. O., Andreae, T. W., and Harriss, R. C.: Regional aerosol chemistry of the Amazon Basin during the dry season, *J. Geophys. Res.*, 93, 1499, doi:10.1029/JD093iD02p01499, 1988.
- 25 Taylor, S. R. and McLennan, S. M.: *The Continental Crust: its Composition and Evolution*, Blackwell Sci., Oxford, UK, 312 pp., 1985.
- Tan, Y., Perri, M. J., Seitzinger, S. P., and Turpin, B. J.: Effects of precursor concentration and acidic sulfate in aqueous glyoxal-OH radical oxidation and implications for secondary organic aerosol, *Environ. Sci. Technol.*, 43, 8105–8112, doi:10.1021/es901742f, 2009.
- 30 Tan, Y., Carlton, A. G., Seitzinger, S. P., and Turpin, B. J.: SOA from methylglyoxal in clouds and wet aerosols: measurement and prediction of key products, *Atmos. Environ.*, 44, 5218–5226, 2010.

Global modeling of
SOA

G. Lin et al.

Title Page

Abstract

Introduction

Conclusions

References

Tables

Figures

◀

▶

◀

▶

Back

Close

Full Screen / Esc

Printer-friendly Version

Interactive Discussion



Tan, Y., Lim, Y. B., Altieri, K. E., Seitzinger, S. P., and Turpin, B. J.: Mechanisms leading to oligomers and SOA through aqueous photooxidation: insights from OH radical oxidation of acetic acid and methylglyoxal, *Atmos. Chem. Phys.*, 12, 801–813, doi:10.5194/acp-12-801-2012, 2012.

5 Volkamer, R., Jimenez, J. L., SanMartini, F., Dzepina, K., Zhang, Q., Salcedo, D., Molina, L. T., Worsnop, D. R., and Molina, M. J.: Secondary organic aerosol formation from anthropogenic air pollution: rapid and higher than expected, *Geophys. Res. Lett.*, 33, L17811, doi:10.1029/2006GL026899, 2006.

10 Volkamer, R., Ziemann, P. J., and Molina, M. J.: Secondary Organic Aerosol Formation from Acetylene (C₂H₂): seed effect on SOA yields due to organic photochemistry in the aerosol aqueous phase, *Atmos. Chem. Phys.*, 9, 1907–1928, doi:10.5194/acp-9-1907-2009, 2009.

Wang, G., Kawamura, K., Umemoto, N., Xie, M., Hu, S., and Wang, Z.: Water-soluble organic compounds in PM_{2.5} and size-segregated aerosols over Mount Tai in North China Plain, *J. Geophys. Res.*, 114, D19208, doi:10.1029/2008JD011390, 2009.

15 Wang, M. H., Penner, J. E., and Liu, X. H.: Coupled IMPACT aerosol and NCAR CAM3 model: evaluation of predicted aerosol number and size distribution, *J. Geophys. Res.*, 114, D06302, doi:10.1029/2008jd010459, 2009.

Warneck, P.: In-cloud chemistry opens pathway to the formation of oxalic acid in the marine atmosphere, *Atmos. Environ.*, 37, 2423–2427, doi:10.1016/S1352-2310(03)00136-5, 2003.

20 Waxman, E. M., Dzepina, K., Ervens, B., Lee-Taylor, J., Aumont, B., Jimenez, J. L., Madronich, S., and Volkamer, R.: Secondary organic aerosol formation from semi- and intermediate-volatility organic compounds and glyoxal: relevance of O/C as a tracer for aqueous multiphase chemistry, *Geophys. Res. Lett.*, 40, 978–982, doi:10.1002/grl.50203, 2013.

25 Xu, K.-M. and Krueger, S. K.: Evaluation of cloudiness parameterizations using a cumulus ensemble model, *Mon. Weather Rev.*, 119, 342–367, doi:10.1175/1520-0493, 1991.

Xu, L. and Penner, J. E.: Global simulations of nitrate and ammonium aerosols and their radiative effects, *Atmos. Chem. Phys.*, 12, 9479–9504, doi:10.5194/acp-12-9479-2012, 2012.

30 Zhang, Q., Jimenez, J. L., Canagaratna, M. R., Allan, J. D., Coe, H., Ulbrich, I., Alfarra, M. R., Takami, A., Middlebrook, A. M., Sun, Y. L., Dzepina, K., Dunlea, E., Docherty, K., DeCarlo, P. F., Salcedo, D., Onasch, T., Jayne, J. T., Miyoshi, T., Shimonono, A., Hatakeyama, S., Takegawa, N., Kondo, Y., Schneider, J., Drewnick, F., Borrmann, S., Weimer, S., Demerjian, K., Williams, P., Bower, K., Bahreini, R., Cottrell, L., Griffin, R. J., Rautiainen, J., Sun, J. Y., Zhang, Y. M., and Worsnop, D. R.: Ubiquity and dominance of oxygenated species in organic

aerosols in anthropogenically-influenced Northern Hemisphere midlatitudes, *Geophys. Res. Lett.*, 34, L13801, doi:10.1029/2007GL029979, 2007.

Zhang, X., Chen, Z. M., and Zhao, Y.: Laboratory simulation for the aqueous OH-oxidation of methyl vinyl ketone and methacrolein: significance to the in-cloud SOA production, *Atmos. Chem. Phys.*, 10, 9551–9561, doi:10.5194/acp-10-9551-2010, 2010.

5

Global modeling of SOA

G. Lin et al.

Title Page

Abstract

Introduction

Conclusions

References

Tables

Figures



Back

Close

Full Screen / Esc

Printer-friendly Version

Interactive Discussion



Table 1. Case descriptions.

Case name	SOA formation in cloud water	SOA formation in aerosol water	Cloud field	Iron chemistry
Case 1	Multiphase reaction scheme is used to predict carboxylic acids and Henry's law is used for all gas/particle transfer. Aqueous phase reactions of organics are adopted from Jacob (1986), Pandis and Seinfeld (1989), Lim et al. (2005), Herrmann (2003), Herrmann et al. (2005), and Carlton et al. (2007) (Table S3 in the Supplement).	Multiphase reaction scheme is used to predict carboxylic acids with the same aqueous phase reactions and gas/particle transfer as in cloud water. Surface-limited uptake process is used to predict oligomers with a reactive uptake parameter of 3.3×10^{-3} for glyoxal and 2.9×10^{-5} for methylglyoxal.	The diagnostic cloud field ^a	N/A
Case 2	The same as in case 1.	Multiphase reaction scheme is used with the aqueous phase reactions proposed by Ervens and Volkamer (2010) (Table S4 in the Supplement).	The diagnostic cloud field ^a	N/A
Case 3	Multiphase reaction scheme is used with the detailed chemistry of Lim et al. (2010) (Table S5 in the Supplement).	Multiphase reaction scheme is used with the detailed chemistry of Lim et al. (2010) (Table S5 in the Supplement).	The diagnostic cloud field ^a	N/A
Case 4	The same as in case 1.	The same as in case 1.	GFDL AM3 cloud field	N/A
Case 5	The same as in case 1, but including aqueous iron chemistry in cloud (Table S6 in the Supplement).	The same as in case 1.	The diagnostic cloud field ^a	Includes aqueous iron chemistry
Case 6	Surface-limited uptake process is used with a reactive uptake parameter of 2.9×10^{-3} for both glyoxal and methylglyoxal.	Surface-limited uptake process is used with a reactive uptake parameter of 2.9×10^{-3} for both glyoxal and methylglyoxal.	The diagnostic cloud field ^a	N/A

^a The diagnostic cloud field used the parameterization for cloud water published by Hack (1998).

Title Page

Abstract

Introduction

Conclusions

References

Tables

Figures

◀

▶

◀

▶

Back

Close

Full Screen / Esc

Printer-friendly Version

Interactive Discussion



Global modeling of SOA

G. Lin et al.

Table 2. Global aqSOA budget analyses for all cases.

Case name	Species name	Chemical production (Tgyr ⁻¹)	Chemical destruction (Tgyr ⁻¹)	Net production (Tgyr ⁻¹)	Dry deposition (Tgyr ⁻¹)	Wet deposition (Tgyr ⁻¹)	Burden (Tg)
Case 1	Glyoxylic acid	8.5	4.0	4.5	0.2	4.3	3.5×10^{-2}
	Pyruvic acid	6.9×10^{-1}	5.1×10^{-1}	1.8×10^{-1}	1.0×10^{-2}	1.8×10^{-1}	1.6×10^{-3}
	Oxalic acid	22.9	7.2	15.7	0.6	15.1	1.0×10^{-1}
	Glyoxal oligomer	6.1	–	6.1	0.4	5.7	8.5×10^{-2}
	Methylglyoxal oligomer	2.2×10^{-1}	–	2.2×10^{-1}	2.4×10^{-2}	2.0×10^{-1}	2.3×10^{-3}
Case 2	Glyoxylic acid	8.7	4.0	4.7	0.2	4.5	3.6×10^{-2}
	Pyruvic acid	6.8×10^{-1}	5.0×10^{-1}	1.8×10^{-1}	8.9×10^{-3}	1.7×10^{-1}	1.5×10^{-3}
	Oxalic acid	23.6	7.3	16.3	0.6	15.7	1.0×10^{-1}
	Glyoxal oligomer	2.5×10^{-2}	–	2.5×10^{-2}	4.4×10^{-3}	2.1×10^{-2}	2.0×10^{-3}
	Methylglyoxal oligomer	1.7×10^{-2}	–	1.7×10^{-2}	4.3×10^{-3}	1.3×10^{-2}	9.7×10^{-4}
Case 3	Glyoxylic acid	8.2	3.7	4.5	0.2	4.3	3.7×10^{-2}
	Pyruvic acid	5.6×10^{-1}	3.9×10^{-1}	1.7×10^{-1}	8.7×10^{-3}	1.6×10^{-1}	1.5×10^{-3}
	Oxalic acid	20.4	6.4	14.0	0.5	13.5	9.1×10^{-2}
	Glyoxal oligomer	4.6×10^{-2}	2.9×10^{-2}	1.7×10^{-2}	5.1×10^{-4}	1.7×10^{-2}	1.8×10^{-3}
	Methylglyoxal oligomer	2.1×10^{-3}	–	2.1×10^{-3}	1.2×10^{-4}	2.0×10^{-3}	1.4×10^{-4}
Case 4	Glyoxylic acid	4.8	3.2	1.6	0.2	1.4	2.6×10^{-2}
	Pyruvic acid	4.4×10^{-1}	3.3×10^{-1}	1.1×10^{-1}	1.0×10^{-2}	1.0×10^{-1}	1.9×10^{-3}
	Oxalic acid	11.8	5.6	6.2	0.4	5.8	8.6×10^{-2}
	Glyoxal oligomer	9.2	–	9.2	0.8	8.3	1.2×10^{-1}
	Methylglyoxal oligomer	4.1×10^{-1}	0	4.1×10^{-1}	5.7×10^{-2}	3.5×10^{-1}	5.2×10^{-3}
Case 5	Glyoxylic acid	12.6	8.3	4.3	0.2	4.1	3.4×10^{-2}
	Pyruvic acid	1.8	1.6	0.2	1.1×10^{-2}	1.9×10^{-1}	1.9×10^{-3}
	Oxalic acid	32.2	27.8	4.4	0.2	4.2	2.4×10^{-2}
	Glyoxal oligomer	5.9	–	5.9	0.4	5.5	8.2×10^{-2}
	Methylglyoxal oligomer	2.3×10^{-1}	–	2.3×10^{-1}	2.5×10^{-2}	0.2	2.3×10^{-3}
Case 6	Glyoxal oligomer	22.6	–	22.6	1.0	21.6	2.0×10^{-1}
	Methylglyoxal oligomer	36.9	–	36.9	1.6	35.3	3.0×10^{-1}



Global modeling of
SOA

G. Lin et al.

Table 3. Global average chemical reactions of organic acids in cloud water for case 1^a.

	Source	Reaction rate (Tgyr ⁻¹)	Sink	Reaction rate (Tgyr ⁻¹)
Glyoxylic acid	Glyoxal + OH/NO ₃	5.1	Reaction with OH	3.7
	Methylglyoxal + OH/NO ₃	6.6 × 10 ⁻²		
	Acetic acid + OH Glycolaldehyde + OH	1.3 2.0	Reaction with NO ₃	3.5 × 10 ⁻¹
Oxalic acid	Glyoxylic acid + OH/NO ₃	4.9	Reaction with OH	4.8
	Glyoxal + OH	17.8	Reaction with NO ₃	1.5
Pyruvic acid	Methylglyoxal + OH	6.8 × 10 ⁻¹	Reaction with OH	5.1 × 10 ⁻¹
	Methylglyoxal + NO ₃	1.8 × 10 ⁻²	Reaction with NO ₃	1.7 × 10 ⁻³

^a Organic acids formed in cloud water account for around 79% of total aqSOA formation rate, while the rest is attributed to the oligomer formation in aerosol water.

Title Page

Abstract

Introduction

Conclusions

References

Tables

Figures

◀

▶

◀

▶

Back

Close

Full Screen / Esc

Printer-friendly Version

Interactive Discussion



Global modeling of
SOA

G. Lin et al.

Title Page

Abstract

Introduction

Conclusions

References

Tables

Figures

◀

▶

◀

▶

Back

Close

Full Screen / Esc

Printer-friendly Version

Interactive Discussion

**Table 4.** Global budgets of aqSOA precursors (Tgyr^{-1}) for case 1.

	Glyoxal	Methylglyoxal	Glycolaldehyde	Acetic Acid
Emission	0	0	0	31.4
Gas phase production	70.5	167.9	81.3	29.3
Aqueous phase production	3.3	0	0	3.6×10^{-1}
Gas phase consumption	44.0	157.7	63.6	25.8
Aqueous phase consumption	23.0	0.86	5.1	1.2
Deposition	6.8	9.3	12.6	34.1

Global modeling of
SOA

G. Lin et al.

Table 5. SOA formation in cloud vs. SOA formation in aerosol water.

	SOA production rate in cloud (Tgyr ⁻¹)	SOA production rate in aerosol water (Tgyr ⁻¹)	Total aqSOA production rate (Tgyr ⁻¹)	Fraction of SOA production in cloud
Case 1	21.1	5.6	26.7	79.0%
Case 2	22.0	-0.9	21.1	104.0%
Case 3	19.5	-0.8	18.7	104.3%
Case 4	8.8	8.7	17.5	50.3%
Case 5	9.5	5.5	15.0	63.3%
Case 6	46.8	12.6	59.4	78.8%

Title Page

Abstract

Introduction

Conclusions

References

Tables

Figures

◀

▶

◀

▶

Back

Close

Full Screen / Esc

Printer-friendly Version

Interactive Discussion



Global modeling of
SOA

G. Lin et al.

Title Page

Abstract

Introduction

Conclusions

References

Tables

Figures

◀

▶

◀

▶

Back

Close

Full Screen / Esc

Printer-friendly Version

Interactive Discussion

**Table 7.** Comparison of simulated OA with observed OA measured in tropical forested regions.

		West Africa (Below 2 km)		Amazon Basin (surface)	Malysian Borneo (surface)
		NO _x (ppt)	SOA ($\mu\text{g m}^{-3}$)	Total OA ($\mu\text{g m}^{-3}$)	Total OA ($\mu\text{g m}^{-3}$)
Observations		210 (Capes et al., 2009)	1.18 (Capes et al., 2009)	0.7 (Chen et al., 2009) 1.70 (Gilardoni et al., 2011)	0.74 (Robinson et al., 2011)
Simulations	case 1	353	2.89	2.56	1.03
	case 2	354	2.62	2.33	0.92
	case 3	352	2.29	2.12	0.92
	case 4	367	2.82	2.48	0.85
	case 5	346	2.36	1.67	0.90
	case 6	352	4.47	4.45	1.57

Global modeling of
SOA

G. Lin et al.

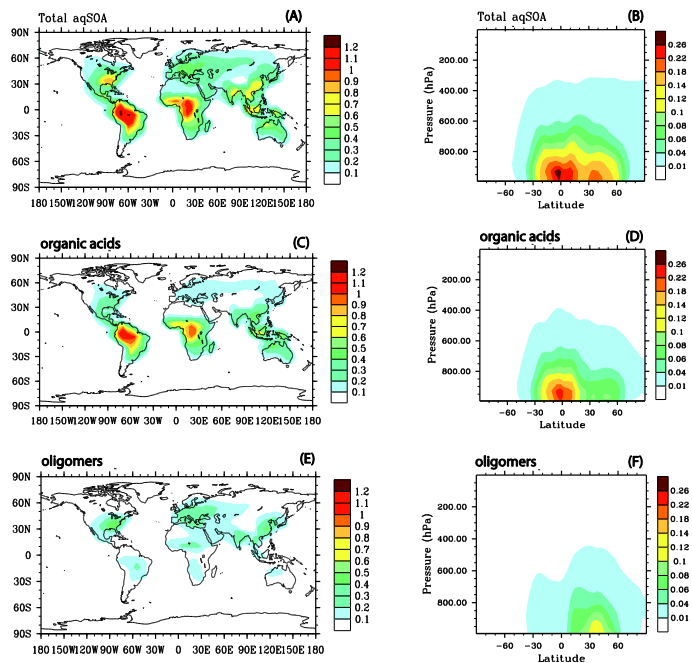


Fig. 1. Annual mean simulated concentrations of total aqSOA (A and B), organic acids (the sum of glyoxylic acid, pyruvic acid and oxalic acid) (C and D), and oligomers from glyoxal and methylglyoxal (E and F). The left column shows the global distributions at the level of 971 hPa in the model; the right column depicts the zonal mean distributions. All plots are for case 1. Units: $\mu\text{g m}^{-3}$.

Full Screen / Esc

Printer-friendly Version

Interactive Discussion



Global modeling of
SOA

G. Lin et al.

Title Page

Abstract

Introduction

Conclusions

References

Tables

Figures

◀

▶

◀

▶

Back

Close

Full Screen / Esc

Printer-friendly Version

Interactive Discussion

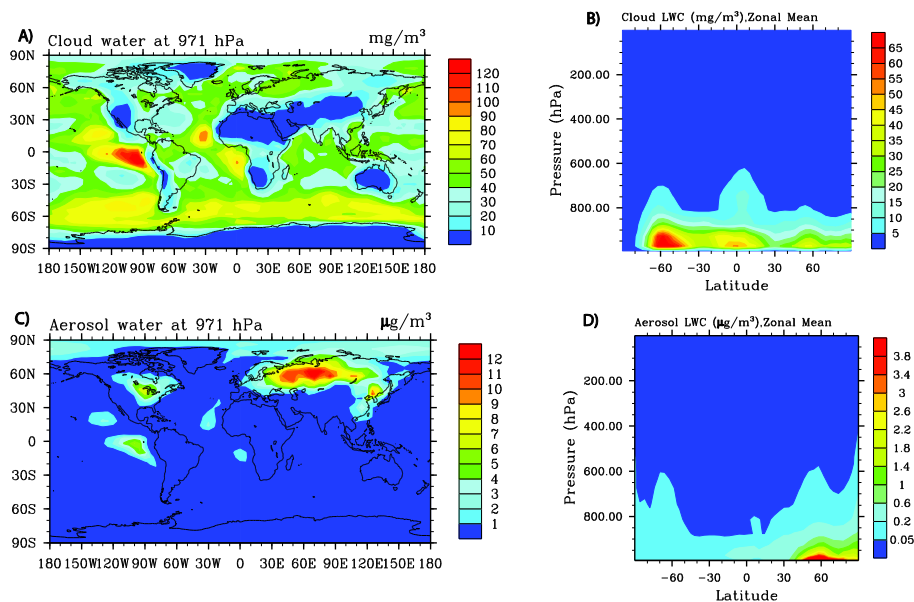


Fig. 2. Annual mean grid-box averaged cloud liquid water content (LWC) in mg/m^3 at approximately 971 hPa (A) and zonal mean content (B), and annual mean aerosol LWC in $\mu\text{g}/\text{m}^3$ at approximately 971 hPa (C) and zonal mean content (D). Plots are for case 1.

Global modeling of
SOA

G. Lin et al.

Title Page

Abstract

Introduction

Conclusions

References

Tables

Figures

◀

▶

◀

▶

Back

Close

Full Screen / Esc

Printer-friendly Version

Interactive Discussion

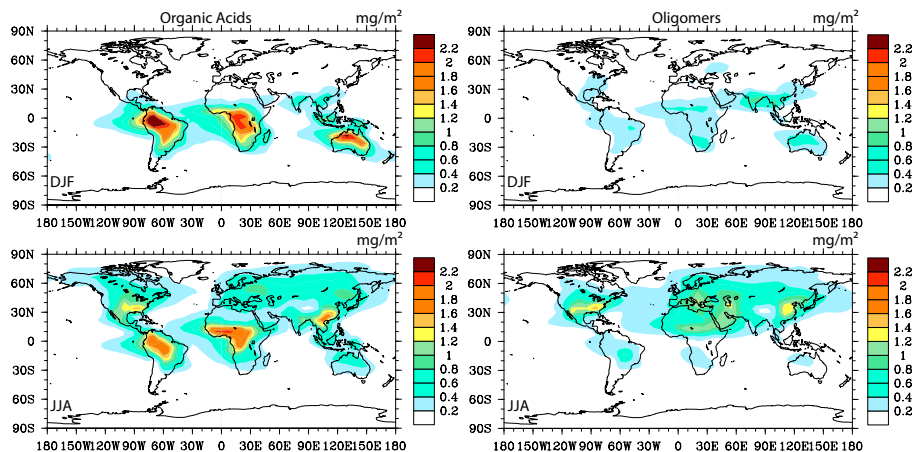


Fig. 3. Seasonally averaged column concentrations (mg m^{-2}) of organic acids (left column) and oligomers (right column) in December, January and February (DJF) (top row) and in June, July and August (JJA) (bottom row). All plots are for case 1.

Global modeling of
SOA

G. Lin et al.

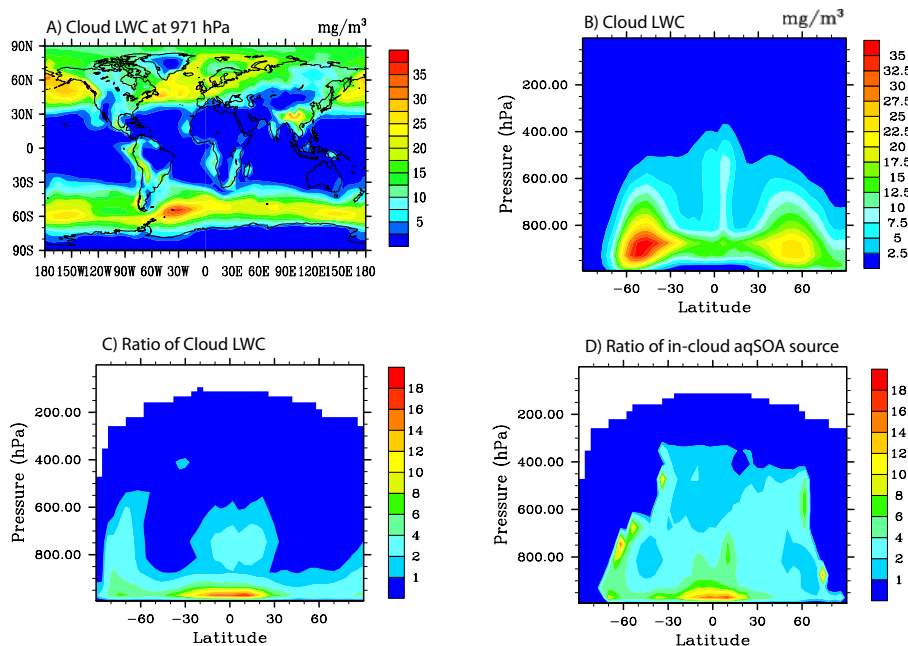


Fig. 4. Annual mean grid-box averaged cloud liquid water content (LWC) in mg/m^3 from the GFDL AM3 cloud field at approximately 971 hPa (**A**) and zonal mean content (**B**) for case 4. (**C**) shows the zonal mean distributions for the ratio of grid-box averaged cloud LWC in case 1 to that in case 4; (**D**) shows the zonal mean distributions for the ratio of the source of aqSOA formed in cloud water in case 1 to that in case 4.

[Title Page](#)[Abstract](#)[Introduction](#)[Conclusions](#)[References](#)[Tables](#)[Figures](#)[◀](#)[▶](#)[◀](#)[▶](#)[Back](#)[Close](#)[Full Screen / Esc](#)[Printer-friendly Version](#)[Interactive Discussion](#)

Global modeling of
SOA

G. Lin et al.

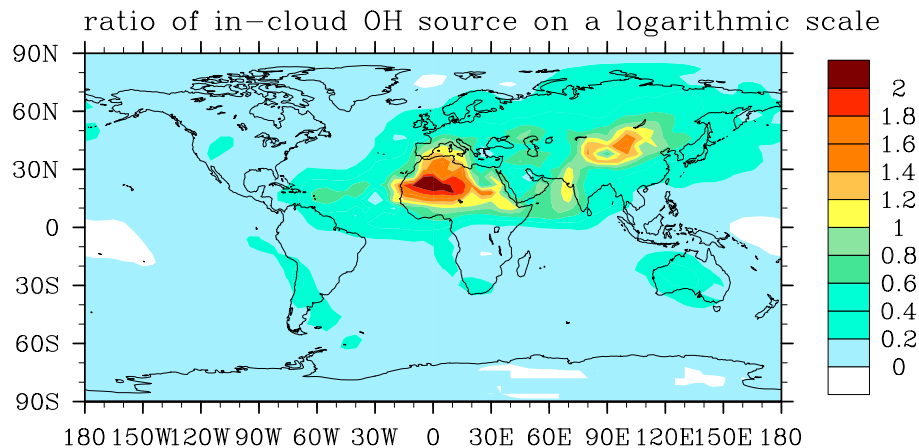


Fig. 5. The ratio of annual mean cloud water OH radical production rates in case 5 (with Fe chemistry) to that in case 1 (without Fe chemistry). The value shown is the logarithm of the ratio.

[Title Page](#)[Abstract](#)[Introduction](#)[Conclusions](#)[References](#)[Tables](#)[Figures](#)[◀](#)[▶](#)[◀](#)[▶](#)[Back](#)[Close](#)[Full Screen / Esc](#)[Printer-friendly Version](#)[Interactive Discussion](#)

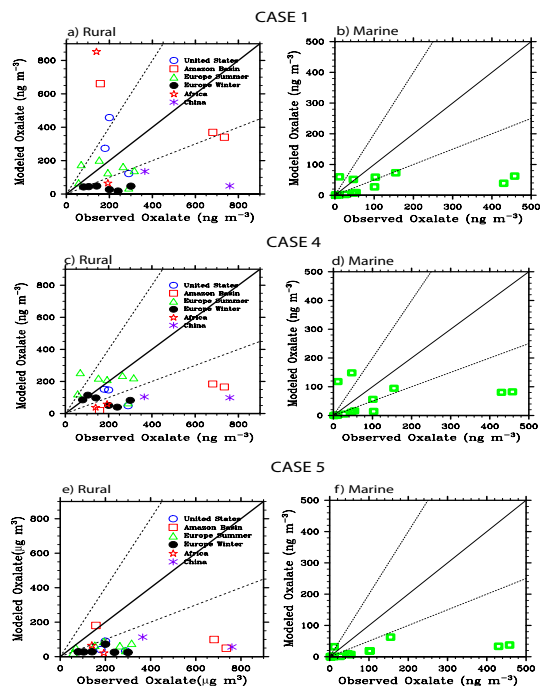


Fig. 6. Comparison of the oxalate mass concentrations observed at rural and marine sites adopted from Table S3 of Myriokefalitakis et al. (2011) with the oxalic acid concentrations simulated in cases 1, 4 and 5. Solid lines show the 1 : 1 ratio, and dashed lines show the 1 : 2 and 2 : 1 ratios. The measurements at the various sites were made in different seasons and different years between 1980 and 2007 and most of them were reported with several days of sampling duration. The model results are the average values over the same months as the observations.

Global modeling of SOA

G. Lin et al.

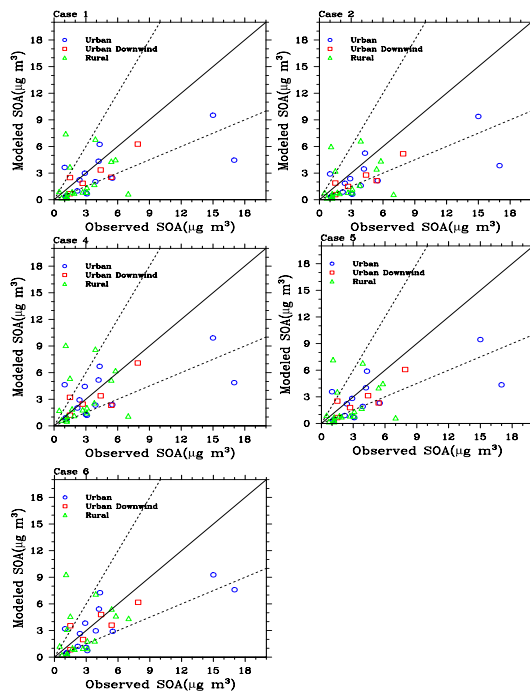


Fig. 7. Comparison of SOA mass concentrations observed at the urban, urban-downwind and rural sites reported in Zhang et al. (2007) with those simulated in case 1, 2, 4, 5 and 6. Solid lines show the 1 : 1 ratio, and dashed lines show the 1 : 2 and 2 : 1 ratios. The measurements at the various sites were made in different seasons and different years between 2000 and 2006 and were reported for the average of different durations spanning from 8 to 36 days. The model results are the average values over the same months as the observations.

[Title Page](#)[Abstract](#)[Introduction](#)[Conclusions](#)[References](#)[Tables](#)[Figures](#)[◀](#)[▶](#)[◀](#)[▶](#)[Back](#)[Close](#)[Full Screen / Esc](#)[Printer-friendly Version](#)[Interactive Discussion](#)

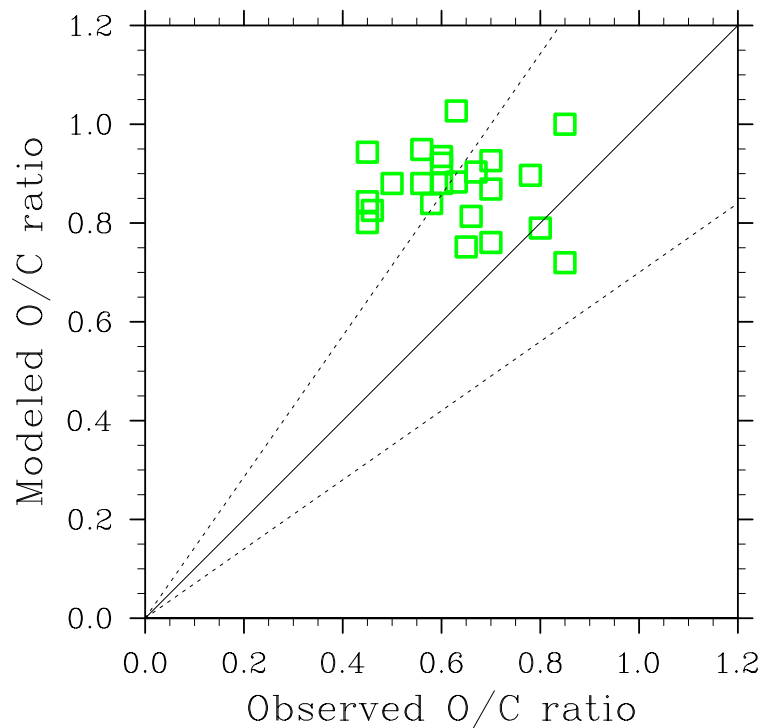


Fig. 8. Comparison of O/C ratio estimated by Ng et al. (2010) for urban downwind, rural and remote sites with those simulated in case 1. The values for other cases are similar to those in case 1. Solid lines show the 1 : 1 ratio, and dashed lines show the 10 : 7 and 7 : 10 ratios, which roughly corresponds to the uncertainty of the AMS measurements, stated as 30 % for the O/C ratio (Aiken et al., 2008). The measurements at the various sites were made in different seasons and different years between 2000 and 2009 and were reported for the average of different durations spanning from 8 to 36 days. The model results are the average values over the same months as the observations.

Title Page	
Abstract	Introduction
Conclusions	References
Tables	Figures
◀	▶
◀	▶
Back	Close
Full Screen / Esc	
Printer-friendly Version	
Interactive Discussion	

